This manuscript was accepted by Renewable Sustainable Energy. Click here to see the version of record.

ANALYSIS OF SOLAR DIRECT IRRADIANCE MODELS UNDER CLEAR-SKIES: EVALUATION OF THE IMPROVEMENTS FOR LOCALLY ADAPTED MODELS

A. Pérez-Burgos[1], M. Díez-Mediavilla[2], C. Alonso-Tristán[2], M.C. Rodríguez-Amigo[2]

(1) Department of Applied Physics, University of Valladolid, Paseo Belén 7, 47011 Valladolid, Spain.
(2) Research Group SWIFT (Solar and Wind Feasibility Technologies), University of Burgos, Avda. Cantabria s/n, 09006 Burgos, Spain.

Corresponding author: Ana Pérez-Burgos Department of Applied Physics, University of Valladolid, Paseo de Belén 7, 47011 Valladolid, Spain.
Email: anapb@uva.es. Phone: +34 983 423749

Abstract

Direct solar irradiance has to be determined for the design of many energy applications such as PV systems, concentration systems and the generation of solar potential maps for energy use. Knowledge of the accurate values of radiation components in a local area will allow optimal sizing of solar energy conversion systems. Estimated values of direct solar irradiance from models are still necessary at those sites where no measurements are available. In this work, different models used for estimation of direct component of solar irradiance are analyzed. Firstly, an evaluation of the performance of eight existing original models was carried out from which three were selected. Secondly, selected models were calibrated to adapt them to our study geographical area and, which is the important aspect of this work, an assessment of performance improvements for locally adapted models is reported. Experimental data consisted of hourly horizontal global, direct and diffuse solar irradiance values, provided by the National Meteorological Agency in Spain (AEMET) for Madrid. Long-term data series, corresponding to a total period of time of 32 years (1980–2011), have been used in this study.

Only clear sky models were treated at the present. The three selected models were adapted to the specific location of Madrid and RMSE and MBE were determined. By comparing the performance in the direct horizontal irradiance estimation from existing original and the corresponding locally adapted models, values of RMSE decreased from 9.9% to 5.7% for the Louche model, from 7.8% to 7.4% for the Robledo-Soler model and finally from 8.8% to 6.7% for the ESRA model. Thus, significant improvements can be reached when parametric models are locally adapted. In our case, it is up to approximately 4% for the Louche model. It is expected that calibrated algorithms presented in this work will be applicable to regions of similar climatic characteristics.

Keywords: solar radiation, direct irradiance, clearness index, diffuse fraction, Linke turbidity factor

I. Introduction

The search for simple, economic energy solutions adapted to local consumption and on a small scale is an emerging need in developed countries [1]. In Spain, as in other European countries, the alternative of "net metering" has been advanced as a solution to the problem of energy supplies [2]. It consists of implementing small installations with mainly renewable energies, which enable self-sufficiency of industrial facilities or residential buildings and grid-connected facilities that exchange energy at times of high and low consumption [3]. This solution prevents distribution losses, increases the reserve capacity and promotes the rational distribution of energy. Photovoltaic (PV) and Concentrated Solar Power (CSP) should be seriously considered as technologies that will help to achieve the goal of universal and cheap electricity produced by high-tech devices that collect solar radiation. A more precise knowledge of the solar radiation components in a local area will imply a more optimal design of its solar systems, for example, PV systems use global irradiances while CSP systems use direct irradiance. An accurate prediction of the energy production of a solar system is not only vital for its integration in the electric grid but also for the consumer.

There are different ways to get the radiation data needed for the calculation of solar facilities such as databases, radiation maps and satellite measurements but, in the majority of cases, these data are not obtained by direct measurement and are not optimal for many localized applications [4]. The models used for the calculation of solar radiation are usually models validated for specific areas and for

This manuscript was accepted by Renewable Sustainable Energy. Click here to see the version of record.

specific geographic and climatic conditions [5]. It is necessary to validate these models and to find adaptations for different conditions and places by adjusting the parameters to the area under study [6].

Several papers deal with the significance of calculating the incident irradiance components under a cloudless sky. Gueymard [7] pointed to the primordial importance of evaluating the maximum solar resource, i.e. the clear-sky direct irradiance, in relation to the use of different energy solar applications particularly those relying on solar concentrators. The importance of clear sky models is mainly because they are a key base for the subsequent application of a cloud factor which leads to irradiance under realistic conditions [8]. The significance of solar radiation models in the Heliosat method is of particular interest as the clear-sky model is a key starting point for subsequent cloudy sky models [9, 10]. In this context, several models have been proposed in the literature [11, 12] so that a previous revision has been carried out in this work.

Global solar irradiance is more commonly measured at radiometric stations than their components, so a number of models were developed to estimate direct or diffuse radiation from the global value. These types of models are called decomposition or separation models [11, 13] as they separate global radiation into its components. Over recent years, a literature search reported 250 such separation methods [11] and different authors have tested the performance of many of these models at different locations and time spans [11, 14-17]. New schemes have recently been proposed [18, 19] to calculate the normal direct irradiance based on the relationship between the diffuse fraction K_d (ratio of diffuse to global irradiance) and the clearness index K_t (ratio of the global irradiance to its corresponding extraterrestrial irradiance) in Europe. Factors that influence direct radiation under cloudless skies are atmospheric turbidity, mainly related to the physicochemical properties of aerosols, and precipitable water content [8]; in specific regions, where turbidity and water vapour show little or no fluctuations, solar geometry is the most important factor that models solar irradiance. So, several empirical models using solar altitude angle as the only input parameter can be found in the literature [20, 21].

In this work, eight solar direct irradiance models based on different types of correlations are analyzed. Decomposition models based on the calculation of the diffuse fraction K_d as a function of the clearness index K_t are often used to calculate the direct component [22] and they will be introduced first. Two types of such algorithms, linear and polynomial, can be found in the literature. Here, a

This manuscript was accepted by Renewable Sustainable Energy. Click here to see the version of record.

representative linear model due to Reindl [23] and two polynomial models due to Erbs [24] and Muneer [25] have been selected. The Erbs model has been recommended in national standards and included as a reference for the performance assessment [26] and the Muneer model provides a correlation which was fitted to the mean global curve based on curves obtained at worldwide locations [27]. Decomposition models based on diffuse fraction calculations continue to be used [17, 22], mainly due to their simplicity.

Models with the solar altitude angle, α, as the only input parameter, are very effective when locally adapted coefficients are applied. In this case, the Robledo-Soler model [21] whose authors proposed coefficients for Madrid has been selected.

The calculation of direct irradiance by using a combination of K_t and α has also been considered. A model also proposed by Reindl et al. [23] which combines both input variables has been included.

Models due to Louche et al. [28] and Maxwell [29] have been also selected. These models, widely cited in literature [13, 17, 27], use the clearness index, K_t, to model the atmospheric transmittance rather than the diffuse fraction. They obtain the direct irradiance by multiplying the transmittance by the extraterrestrial irradiance.

Finally, the clear sky model used by Ref. [9], the ESRA (European Solar Radiation Atlas) model was selected. The Linke turbidity factor is a key input parameter in this model. For clear days, the Linke factor is, mainly, a function of aerosols and water vapour content. This factor, typically varies from 3 (clear days) to 7 (heavily polluted skies) [30]. Knowledge of this factor in a given location and time is needed for accurate predictions from the ESRA model. Taking this into account, the Linke factor was determined for the location under study.

The eight studied models are referred in this work as Reindl1 model, Erbs model, Muneer model, Louche model, Reindl2 model, Robledo-Soler model, Maxwell model and ESRA model.

This paper is organized as follows: Climatic conditions and experimental data are described in section II; the performance of eight clear-sky direct irradiance models is evaluated in section III; this section is carried out in three steps: firstly, the selection of clear sky data is described, secondly, the

125 mathematical equations of the eight selected models are shown and thirdly, the performances of the
126 models are analyzed using statistical errors –mean-biased error (MBE) and root mean square error
127 (RMSE). In section IV, three best-performance selected models are calibrated using data from a
128 specific location, Madrid. The improvement of the predictions between parametric models locally
129 adapted with respect to their original formulations is quantified. Final remarks and conclusions are
130 provided in section V.
131
132 **II. Climatic conditions and experimental data**
133
134 Madrid has a Mediterranean continental climate characteristic of the much of Spain's inland territory,
135 where continental features are due to the limited influence of the sea. This type of climate is
136 characterized by wide diurnal and seasonal variations in temperature and by low and irregular rainfall.
137 Continental winters are cold and summers are warm and cloudless. Figure 1 shows the annual
138 evolution of mean values of temperature and rainfall at Madrid for the period 1981-2010
139 (http://www.aemet.es/es/). Temperature varies from 25.6 ºC in July to 6.3 ºC in January and rainfall
140 varies from 60 mm in October to 10 mm in August. It is expected that the results from this study will
141 be applicable to regions of similar climatic characteristics [31].
142

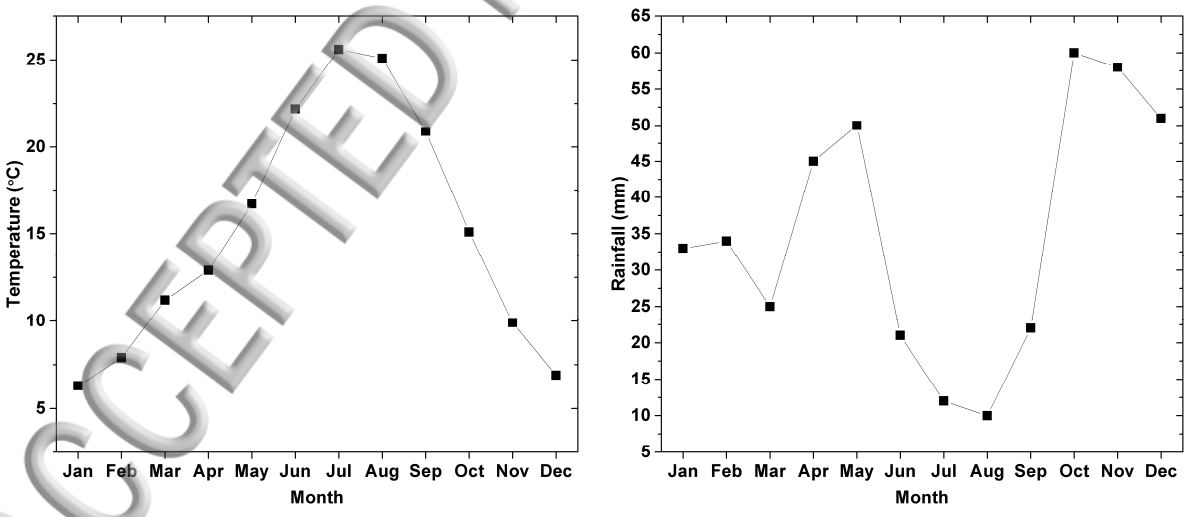

143
144
145 **Figure 1.** Climatic values (time period 1981-2010) of temperature and rainfall for each month at
146 Madrid (Data obtained from AEMET)

This manuscript was accepted by Renewable Sustainable Energy. Click here to see the version of record.

Experimental data used in this work consist of measurements of global, diffuse and direct irradiance on a horizontal surface provided by the National Meteorological Agency (AEMET) from the radiometric station sited in Madrid [32]; its geographical coordinates, latitude and longitude, are 40°27' N, 3°43' W at an elevation of 663 meters above sea level. Data on a hourly basis have been managed corresponding to complete years for the period 1980-2011; data from 1980 to 2004 were used for model selection and from 2005 to 2011 were used for intercomparisons between original and locally adapted models. Data from 5:00h to 20:00h were available for each day, the irradiance value at a specific time corresponds to an average over the hour before. Time is expressed in True Solar Time (TST). Global and diffuse radiation data were obtained from bimetallic sensors SIAP until 1983, Kipp & Zonen CM5 until May 1995, Kipp & Zonen CM11 until December 2004 and Kipp & Zonen CM21 from 2005. Data of direct radiation have been measured by direct sensors Eppley NIP until December 2004 and Kipp & Zonen CH-1 from 2005. Diffuse sensors were installed on shadow bands and directly over conventional solar trackers (Eppley) until 2001 and from this date, an automatic solar trackers Kipp & Zonen 2AP model has been used. Each sensor is calibrated bi-annually at the National Radiation Centre in Madrid, with reference to a standard pyranometer or pyrheliometer directly referenced to WSG Davos. The AEMET radiometric network has the certification ISO 9001:2000.

III. Performance of models

The objective of this section is to categorize our data into different sky conditions and to evaluate the performance of eight models to calculate clear sky direct horizontal irradiance. A set of 25 years of data corresponding to the period 1980-2004 has been used in this study. The selection of clear sky data is described in subsection III.A. The description of models is made in section III.B and the comparison of models performance is carried out in section III.C.

A. Selection of clear sky data

A classification of data into different sky conditions was done previous the application of models. In order to select clear sky data, different criteria have been proposed in the literature including sky ratio,

This manuscript was accepted by Renewable Sustainable Energy. Click here to see the version of record.

178 cloud cover, Perez sky clearness index and clearness index between others [27, 33, 34]. We have
179 applied two of them, one is the clearness index, K_t; this index is commonly used due to it is based on
180 the most accessible solar radiation measurement which is horizontal global irradiance [33]. K_t is also
181 used as input parameter in some of the studied models; the other is the more sophisticated Perez
182 clearness index, proposed initially into the Perez model [14] and valued by its high accuracy [33].
183 The Perez sky clearness index, ε, is defined [14] :

184
$$\varepsilon = \frac{\frac{D_h + B_n}{D_h} + k\theta^3}{1 + k\theta^3} \qquad (1)$$

185 where, D_h is the horizontal diffuse irradiance, B_n, the normal direct irradiance, θ, the solar zenith angle
186 in radians and k, a constant equal to 1.041. Eight categories of cloudiness are defined depending on
187 the value of the ε. Category 1 corresponds to totally overcast and category 8 to totally clear skies. A
188 simplified classification of the values of ε in three categories, overcast, intermediate and clear skies is
189 given in Table I.
190
191 **Table I.** Range of values of the Perez sky clearness index ε for three sky conditions, overcast,
192 intermediate and clear sky.

Bin no.	Sky conditions	ε
1-2	Overcast skies	1-1.23
3-6	Intermediate skies	1.23-4.5
7-8	Clear skies	4.5-

193
194
195 In this study, a lower limit to select clear-sky data was established at $\varepsilon=5$ [35], corresponding to
196 category 8 and a part of 7. The clearness index K_t [8] is expressed by:
197
198
$$K_t = {}^{G_h}\!/_{I_0 \cdot \sin\alpha} \qquad (2)$$

199
200 where G_h is the global horizontal irradiance and I_0 the extraterrestrial irradiance normal to the solar
201 beam defined as $I_0 = I_{sc} E_o$ being I_{sc}, the solar constant and E_0, the correction factor for the sun-earth
202 distance calculated by [29]:

This manuscript was accepted by Renewable Sustainable Energy. Click here to see the version of record.

$$E_0 = 1.00011 + 0.034221 \cdot \cos(\Gamma) + 0.001280 \cdot \sin(\Gamma) + 0.000719 \cdot \cos(2 \cdot \Gamma) + 0.000077 \cdot \sin(2 \cdot \Gamma)) \quad (3)$$

where, Γ, the day angle, is given for each day of the year, J, by:

$$\Gamma = \frac{2 \cdot \pi \cdot J}{365.25} \quad (4)$$

A lower value of K_t=*0.6* to select clear skies [36, 37] has been also tested in the present work as will be described below.

In Figure 2, a classification of data based on the Perez index ε is shown. Values of global and direct horizontal irradiance averaged for each category are presented for a period of 25 years, 1980-2004. From this figure, it can be seen, that the proportion of the direct to global horizontal irradiance increases when cloudiness decreases, as expected.

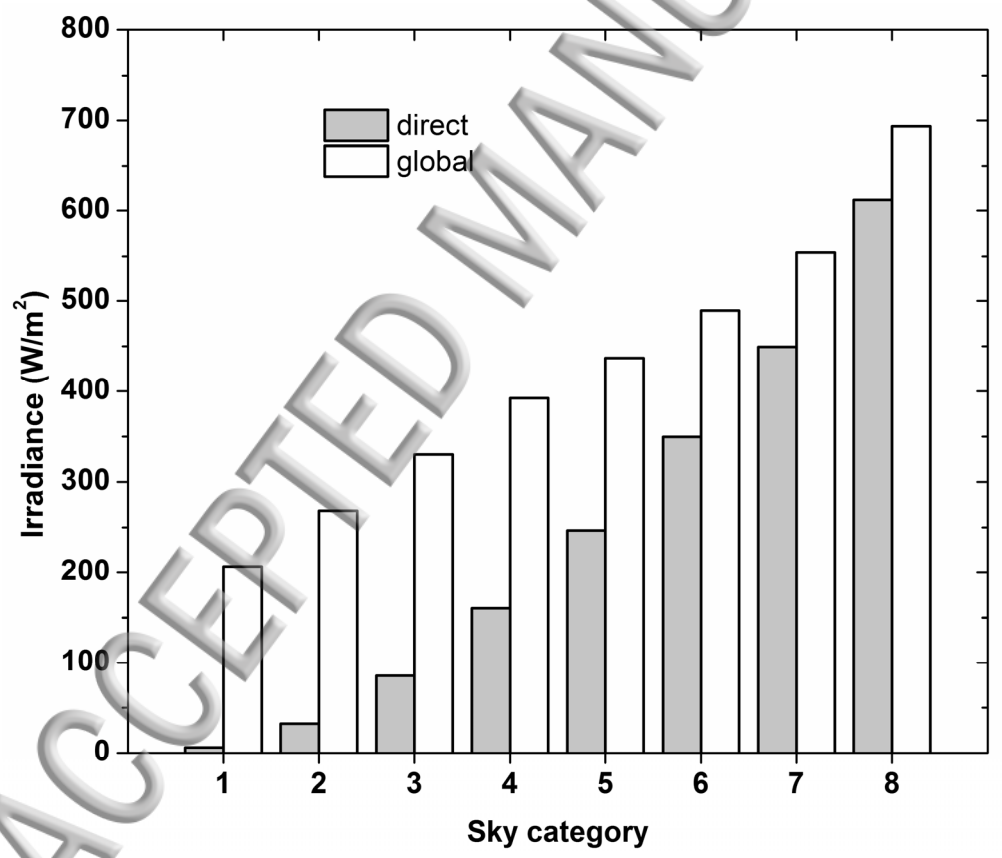

Figure 2. Mean global and direct horizontal irradiances for each sky category (based on the Perez's index ε) at Madrid for the time period 1980-2004.

This manuscript was accepted by Renewable Sustainable Energy. Click here to see the version of record.

When the condition ε>5 is applied, 32% of the whole data are selected as clear-sky data; in case of applying the condition K_t>0.6, 60% of data are selected. It is clear that the first condition is more restrictive. Nevertheless, when applied K_t>0.6 over the selection made based on ε, 1% of data were removed at higher. Thus, 31% of the whole data set was selected as clear sky data and used in this work. As the percentage does not appreciably change, conclusions would be similar if only the criterion based on ε is applied.

B. Description of models

With regards to diffuse fraction models, these are based on the relationship K_d-K_t as described in section I; this type of models is still used to estimate horizontal direct irradiance as indicated by recent papers [22, 38]. The clearness index K_t has been already defined by the expression (2); the diffuse fraction is defined as:

$$K_d = D_h / G_h \qquad (5)$$

where, G_h and D_h are the global and diffuse horizontal irradiances, respectively. K_d -K_t models were initially proposed to calculate diffuse irradiance; however, numerous authors [15, 18, 26] have taken advantage of these models to calculate direct irradiance; Following this idea, in this work, the direct horizontal irradiance B_h is obtained by making the difference between the global and diffuse irradiance, i.e.:

$$B_h = G_h - D_h = G_h - G_h K_d = G_h(1 - K_d) \qquad (6)$$

For these types of models as well as for the other models selected (described in section I), the mathematical algorithms are given as follows:

a) Reindl1 Model [23]

$$B_h = G_h \cdot (1 - K_d)$$

$$\begin{aligned} K_d &= 1.020 - 0.248 \cdot K_t & K_t &\le 0.30 \\ K_d &= 1.450 - 1.670 \cdot K_t & 0.30 < K_t &< 0.78 \\ K_d &= 0.147 & K_t &\ge 0.78 \end{aligned} \qquad (7)$$

This manuscript was accepted by Renewable Sustainable Energy. Click here to see the version of record.

247

248 b) *Erbs Model* [24]

249 $$B_h = G_h \cdot (1 - K_d)$$

$$K_d = 1.0 - 0.09K_t \qquad K_t \le 0.22$$

250 $$K_d = 0.9511 - 0.1604 \cdot K_t + 4.388 \cdot K_t^2 - 16.638 \cdot K_t^3 + 12.336 \cdot K_t^4 \qquad 0.22 < K_t \le 0.8 \qquad (8)$$

$$K_d = 0.165 \qquad K_t > 0.8$$

251

252 c) *Muneer Model* [25]

253 $$B_h = G_h \cdot (1 - K_d)$$

254 $$K_d = 1.006 - 0.317 \cdot K_t + 3.1241 \cdot K_t^2 - 12.7616 \cdot K_t^3 + 9.7166 \cdot K_t^4 \qquad (9)$$

255

256 d) Louche Model [28]

257 $$B_h = K_b \cdot I_0 \cdot \sin\alpha$$

258 K_b is the atmospheric direct transmittance given by:

259 $$K_b = 0.002 - 0.059 \cdot K_t + 0.994 \cdot K_t^2 - 5.205 \cdot K_t^3 + 15.307 \cdot K_t^4 - 10.627 \cdot K_t^5 \qquad (10)$$

260

261 e) *Reindl 2 Model* [23]

262 $$B_h = G_h \cdot (1 - K_d)$$

$$K_d = 1.020 - 0.254 \cdot K_t + 0.0123 \cdot \sin\alpha \qquad K_t \le 0.30$$

263 $$K_d = 1.400 - 1.749 \cdot K_t + 0.177 \cdot \sin\alpha \qquad 0.30 < K_t < 0.78 \qquad (11)$$

$$K_d = 0.486 \cdot K_t - 0.182 \cdot \sin\alpha \qquad K_t \ge 0.78$$

264

265 f) *Robledo-SolerModel* [21]

266 $$B_h = 1201.87 \cdot (\sin\alpha)^{1.346} e^{-0.0041 \cdot \alpha} \qquad (12)$$

267

268 g) *Maxwell Model* [29]

269 $$B_h = I_0 \cdot \sin\alpha \cdot \left(K_{nc} - (A + B \cdot \exp(m \cdot C))\right) \qquad (13)$$

270 In eq. (13), the expression between brackets is the direct transmittance, K_n, where:

271 $$K_{nc} = 0.866 - 0.122 \cdot m + 0.0121 \cdot m^2 - 0.000653 \cdot m^3 + 0.000014 \cdot m^4 \qquad (14)$$

272 m is the relative optical air mass and A, B, C are coefficients which for $K_t > 0.6$ are given by:

This manuscript was accepted by Renewable Sustainable Energy. Click here to see the version of record.

$$A = -5.743 + 21.77 \cdot K_t - 27.49 \cdot K_t^2 + 11.56 \cdot K_t^3$$
$$B = 41.40 - 118.5 \cdot K_t + 66.05 \cdot K_t^2 + 31.90 \cdot K_t^3 \quad (15)$$
$$C = -47.01 + 184.2 \cdot K_t - 222.0 \cdot K_t^2 + 73.81 \cdot K_t^3$$

h) Clear-sky ESRA model [9]

A different scheme from those described above is provided by the ESRA model that refers to atmospheric turbidity parameters to estimate irradiance. This method has been evaluated in numerous works [39-41] and shows an acceptable response comparable to that of the most sophisticated models. The clear sky ESRA algorithm is given by:

$$B_h = I_0 \cdot \sin\alpha \ \exp(-0.8662 \cdot \delta_R \cdot m \cdot T_{Lm2}) \quad (16)$$

T_{Lm2} is the Linke turbidity factor for an air mass equal to 2, m is the relative optical air mass and δ_R is the Rayleigh optical depth at air mass m. The exponential part in eq. (16) represents the transmittance of the direct radiation under clear skies. All the variation of this transmittance with air mass is included in the product $m\delta_R(m)$ [9]; T_{Lm2} is a normalized Linke factor independent of the air mass that has been introduced in many European models[41]. δ_R is calculated [42] by the expression:

$$\delta_R = 1.0 / (6.6296 + 1.7513 \cdot m - 0.1202 \cdot m^2 + 0.0065 \cdot m^3 - 0.00013 \cdot m^4) \quad (17)$$

m is calculated by [42]:

$$m = \frac{p}{p_0} \cdot \frac{1}{\sin\alpha + 0.50572 \cdot (\alpha + 6.07995)^{-1.6364}} \quad (18)$$

The correction pressure factor is given by:

$$\frac{p}{p_0} = \exp\left(\frac{-z}{8435.2}\right) \quad (19)$$

p_0 is the standard pressure, 1013.25 mb and z=663 m is the height for Madrid,

C. Comparison of the models

Models described in section III.B were applied to the clear sky data selected from a period of 25 years (1980-2004). Estimated and measured values of direct horizontal irradiance are compared in Figure 3(a-h). In the case of the ESRA model, it does not have empirical coefficients but its accuracy

300 depends on the appropriate knowledge of T_{Lm2} at the site. Values of T_{Lm2} for Madrid were taken from
301 Remund et al. [43] consisting of monthly values generated in the Solar Radiation Data (SODA)
302 project for the period 1981-1990. In graphs of Figure 3, line 1:1 is depicted for each model. The
303 number of pairs of data used in the comparison is 23229. A first impression about models
304 performance can be obtained from these graphs. Thus, the models based on the diffuse fraction,
305 Reindl 1, Reindl 2, Erbs and Muneer underestimate the measured values. In the case of Maxwell
306 model, deviations depend on the value of irradiance; higher errors are expected for higher irradiance
307 values. For the rest of models, lower errors are obtained.

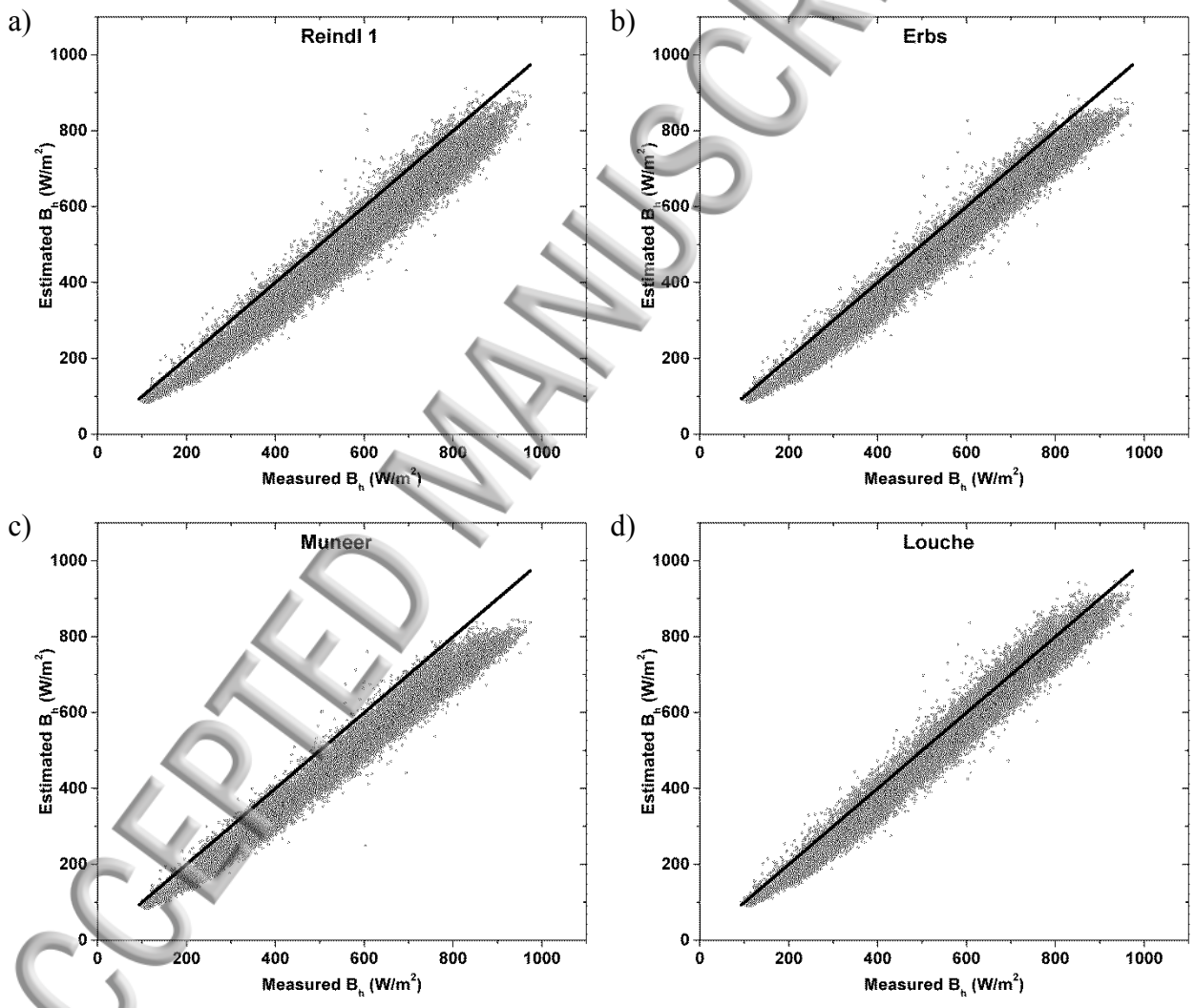

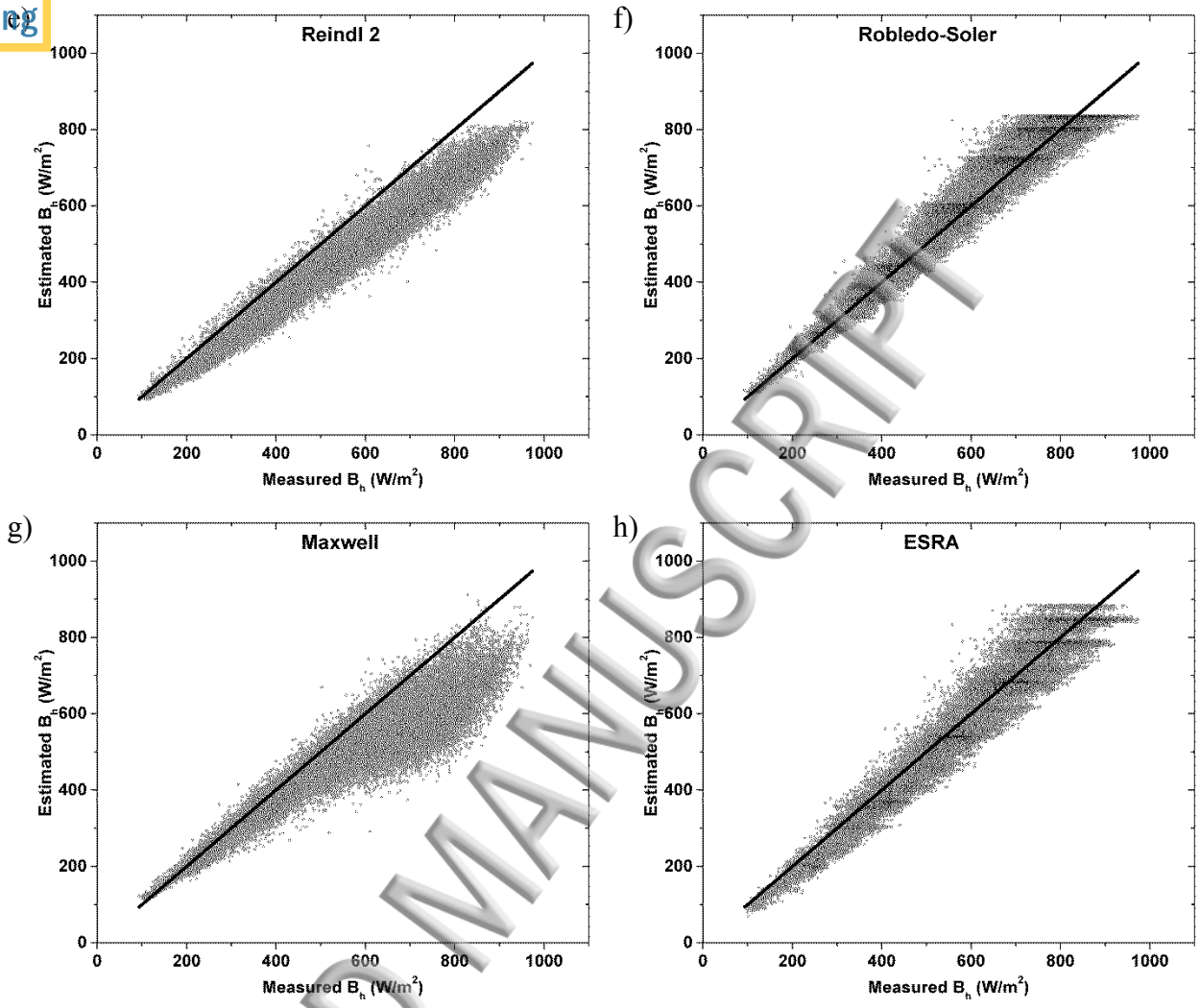

Figure 3. Estimated values of clear-sky direct horizontal irradiance against the corresponding measured values for the eight models analyzed in section III.B for the time period 1980-2004. Solid black line represents the 1:1 relationship.

308 Two statistical indicators are used to test the performance of the models [44], the root mean square
309 error (RMSE) and the mean bias error (MBE). These indicators, defined as relative percentages of the
310 mean value, are calculated by the expressions:
311

This manuscript was accepted by Renewable Sustainable Energy. Click here to see the version of record.

$$RMSE(\%) = \frac{100}{\langle M_i \rangle}\sqrt{\frac{1}{N}\sum_{i=1}^{N}(E_i - M_i)^2}$$
$$MBE(\%) = \frac{100}{\langle M_i \rangle}\frac{1}{N}\sum_{i=1}^{N}(E_i - M_i) \quad (20)$$

where, E_i and M_i are the estimated and measured values, respectively, $\langle M_i \rangle$ is the mean value of the measured values, and N is the total number of data in the comparison process.

Four ranges of solar altitude angles have been taken to evaluate each model. In Table II, the number of data and the mean value of radiation, obtained from the measured data, in each range are shown as well as the values corresponding to the whole range. In Table III, the values of MBE and RMSE are given for each model and for each solar altitude angles range.

Table II. Number of data (N) and mean direct horizontal irradiance from measured data at Madrid for different solar altitude angle ranges and for the total of data for the period 1980-2004.

α	<20º	20º-40º	40º-60º	>60º	Total
N	1526	8180	8646	4877	23229
Mean B_h (W/m^2)	208.29	416.09	653.97	800.79	571.75

Table III. Performance of the eight analyzed models in section III.B for different solar altitude angle ranges and the total data based on the time period 1980-2004 at Madrid.

		MBE(%)					RMSE(%)				
Model	α	<20º	20º-40º	40º-60º	>60º	Total	<20º	20º-40º	40º-60º	>60º	Total
Reindl 1		-19.18	-14.14	-11.06	-9.38	-11.55	22.1	16.2	12.53	10.51	13.23
Erbs		-15.85	-11.3	-8.72	-7.4	-9.17	19.3	13.23	10	8.57	10.71
Muneer		-18.07	-14.45	-12.23	-11.04	-12.59	20.79	15.79	13.1	11.85	13.84
Louche		-11.79	-7.13	-4.37	-2.94	-4.83	16.18	10.32	6.88	5.32	7.54
Robledo-Soler		-0.07	0.48	2.6	1.1	1.55	7.93	7.8	7.68	7.23	7.88
Reindl 2		-13.25	-13.54	-14.91	-15.65	-14.74	17.2	15.73	15.93	16.32	16.79
Maxwell		-1.24	-4.66	-13.32	-22.06	-13.38	7.24	8.66	15.8	23.19	18.91
ESRA		-13.12	-6.59	-1.63	1.25	-2.33	16.15	10.82	7.8	7.48	8.76

This manuscript was accepted by Renewable Sustainable Energy. Click here to see the version of record.

328

329

330 RMSE values in Table III show that the best performance models are Maxwell at the solar altitude
331 angles α <20º, Robledo-Soler at the range 20º-40º and Louche at α >40º.The highest errors may be
332 seen in the Reindl 2 and the Maxwell model; in the case of the Maxwell model, the errors are low for
333 low solar altitude angles but increase as this parameter rises; the rest of the models have low errors
334 with RMSE ranging, approximately, between 8 and 14% for the whole data set; slight variations of
335 these numbers can be found within each solar altitude angle range. The lowest RMSE is obtained for
336 the Louche model. Regarding to MBE, very small values are obtained in the case of the Robledo-Soler
337 and the ESRA models, indicating no tendency towards under or overestimation. The rest of the
338 models have, in most cases, a tendency towards underestimation. As a conclusion, the Louche, the
339 Robledo-Soler and the ESRA models show the best performance. Models based on the K_d-K_t
340 relationship (Reindl 1, Erbs and Munner) have higher errors, although their RMSE values are below
341 14%.
342 Table IV shows the performance of the eight models but using data corresponding to the period of
343 years 2005-2011. By comparing Table III and Table IV, some conclusions can be obtained; firstly, it
344 can be seen that the number of years used in the sample affects the results; thus, Table IV shows
345 higher errors due to the smaller data set used in this case of only seven years; however, some models
346 are not so affected as others. Specifically, Robledo-Soler and ESRA model do not significantly
347 modify their total RMSE values when the time period of data changes. Secondly, concerning to the
348 overall models performance, conclusions for Table IV are the same as those described for Table III
349 and Louche, Robledo-Soler and ESRA models show also in Table IV the best performance.
350
351
352 **Table IV.** Performance of the eight analyzed models in section III.B for different solar altitude angle
353 ranges and the total data based on the time period 2005-2011 at Madrid.

		MBE(%)					RMSE(%)				
Model	α	<20º	20º-40º	40º-60º	>60º	Total	<20º	20º-40º	40º-60º	>60º	Total
Reindl 1		-24.09	-20.32	-13.71	-11.54	-15.13	26.16	21.31	14.62	12.32	16.16
Erbs		-20.79	-16.80	-11.08	-9.53	-12.43	23.33	17.92	11.93	10.30	13.44
Muneer		-22.57	-19.62	-14.49	-13.11	-15.69	24.77	20.51	15.12	13.67	16.60

Louche	-16.90	-13.09	-6.96	-5.20	-8.37	19.90	14.59	8.39	6.58	9.88
Robledo-Soler	2.70	-2.47	1.45	-2.68	-1.67	8.11	8.10	7.39	7.30	7.81
Reindl 2	-18.50	-18.92	-17.03	-17.73	-17.79	21.14	20.10	17.81	18.23	19.32
Maxwell	-3.11	-9.70	-15.94	-24.39	-16.43	10.01	12.02	17.67	25.24	21.12
ESRA	-17.29	-8.22	-3.61	-1.12	-4.49	18.99	11.10	7.81	6.87	8.75

Our interest in this point is the selection of the models with the best performance. Regarding this, the same conclusions can be obtained from both tables. Thus, those algorithms found to have the best performance (Louche, Robledo-Soler and ESRA) were selected for further analysis that will consist in the obtaining of new models parameters adapted to the studied area.

IV. Calibration of models

In order to improve the performance of the models selected in subsection III.C, a local adaptation to a specific site, Madrid, has been carried out. In first place, empirical coefficients were recalculated with data from Madrid for the Louche and the Robledo-Soler algorithms. Regression analyses were performed on algorithms (10) and (12) to obtain new coefficients. Data for the time period 1980-2004 were used in the fitting process. The obtained equations are:

Louche model:

$$K_b = 1.635 - 4.440 \cdot K_t + 2.455 \cdot K_t^{\,2} + 3.876 \cdot K_t^{\,3} + 0.646 \cdot K_t^{\,4} - 3.673 \cdot K_t^{\,5} \quad (21)$$

with R^2=0.71

Robledo-Soler model:

$$B_h = 1092.475 \cdot (\sin \alpha)^{1.276} \cdot e^{-0.0030 \cdot \alpha} \quad (22)$$

with R^2=0.97

In the case of Robledo-Soler, their model was originally established for Madrid; therefore, calibrated and original coefficients are close. Nevertheless, greater reliability is achieved here, as the new

This manuscript was accepted by Renewable Sustainable Energy. Click here to see the version of record.

coefficients were calculated over a lengthy time span of 25 years while original ones were obtained over a time period of 18 months, June 1994 to November 1995.

The treatment in the case of the ESRA model was different. As mentioned above, the accuracy on the outputs from the expression (16) is directly related with the accuracy in T_{Lm2}, therefore, this input parameter should be assessed at each site on a climatological basis, season by season [9]. Thus, the following part of this section is dedicated to the retrieval of more realistic values of T_{Lm2} for Madrid:

Calculation of the Linke Factor T_{Lm2} for Madrid

Values of T_{Lm2} were calculated for Madrid on a hourly basis for the period 1980-2004. This was done through eq. (16) solving for this factor:

$$T_{Lm2} = \ln\left(\frac{B_h}{I_0 \cdot \sin\alpha}\right) \Big/ \left(-0.8662 \cdot \delta_R \cdot m\right) \qquad (23)$$

by using the measured direct horizontal irradiance B_h in this period of time as input [39]. Several representative statistical averages for T_{Lm2} were obtained from those hourly values. First, daily values were calculated; these are represented as points in Figure 4. These daily values were used to calibrate the climatological Bourges algorithm [45] that accounts for the annual variation of turbidity [10].

$$T_{Lm2} = T_0 + u\cos(\Gamma) + v\sin(\Gamma) \qquad (24)$$

where, Γ is the day angle redefined using the eq. (4) and T_0, u and v are local empirical coefficients to be determined for Madrid. A regression analysis was carried out over the aforementioned data period. The coefficients obtained for Madrid were:

$$T_0 = 3.25 \qquad u = -0.52 \qquad v = -0.06 \qquad (25)$$

with a coefficient of determination of R^2=0.86. The fitting analysis is graphically shown in Figure 4, where the points represent the averaged measured values of T_{Lm2} for each day number of the year and the line corresponds to the values predicted by the Bourges algorithm.

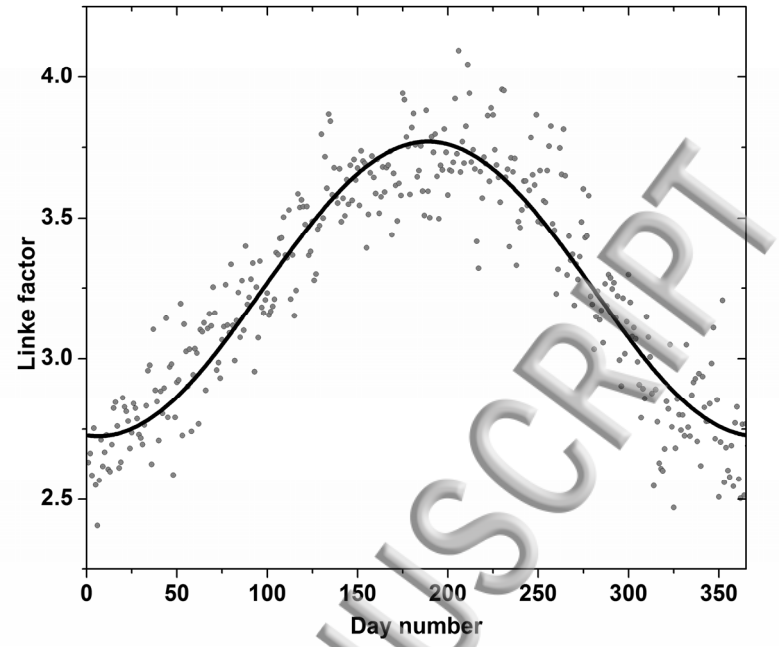

Figure 4. Daily average values of T_{Lm2} (points on the graph) obtained from experimental data and polynomial regression curve (black solid line) corresponding to estimated values from the Bourges algorithm with coefficients obtained for Madrid for the time period 1980-2004.

Secondly, monthly mean hourly values of T_{Lm2} were obtained. This type of averaged values has been very useful in different solar radiation studies [46, 47] as they represent typical climatic behavior. These values are shown in Table V. For any month, T_{Lm2} increases as the hour increases, reaching a maximum at 12h-13h and then decreases with hours thereafter. Typical behavior is illustrated in Figure 5 which shows the variation of T_{Lm2} with time of day for the month of June. Table V also indicates that, at any hour, T_{Lm2} increases with month, reaching a maximum in July and decreases thereafter. Typical behaviour is illustrated in Figure 6 which shows the variation of T_{Lm2} with months of the year at 12h. A variation range for T_{Lm2} between 2.4 and 4 can be established for the overall data.

Table V. Monthly mean hourly values of the Linke Factor T_{Lm2} at Madrid calculated over the period of time1980-2004 from experimental data of direct horizontal irradiance.

Hours	Jan	Feb	Mar	Apr	May	Jun	Jul	Aug	Sep	Oct	Nov	Dec
5												
6												
7				2.54	2.74	2.77	2.76	2.61				
8		2.38	2.68	2.83	3.02	3.12	3.14	3.02	2.81	2.59		
9	2.45	2.65	2.86	3.07	3.33	3.48	3.49	3.36	3.16	2.84	2.52	2.63
10	2.64	2.78	3.10	3.32	3.62	3.73	3.77	3.67	3.49	3.13	2.70	2.62
11	2.77	2.95	3.25	3.48	3.79	3.92	3.98	3.89	3.77	3.31	2.86	2.75
12	2.83	3.08	3.33	3.58	3.92	4.02	4.06	3.97	3.85	3.46	3.01	2.81
13	2.81	3.09	3.28	3.57	3.90	3.96	4.03	3.92	3.78	3.42	2.95	2.86
14	2.76	2.97	3.24	3.46	3.77	3.80	3.85	3.79	3.66	3.31	2.88	2.77
15	2.62	2.80	3.10	3.33	3.59	3.65	3.70	3.53	3.44	3.11	2.75	2.63
16	2.38	2.65	2.84	3.02	3.34	3.40	3.44	3.21	3.18	2.82	2.54	2.52
17		2.60	2.70	2.81	3.06	3.09	3.12	2.97	2.90	2.55		
18				2.43	2.79	2.77	2.79	2.73				
19												
20												

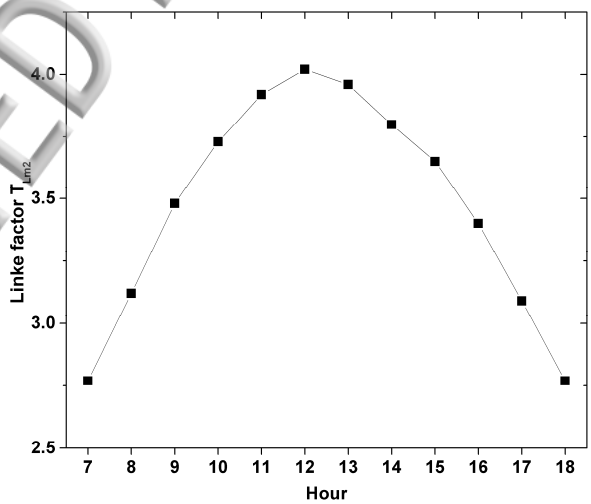

Figure 5. Variation of T_{Lm2} with time of day for the month of June at Madrid based on the period of time 1980-2004

434

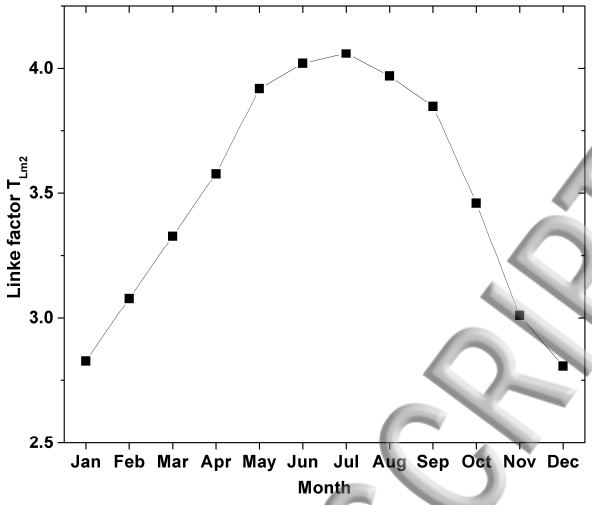

435

436 **Figure 6.** Variation of T_{Lm2} with month of year at 12h at Madrid based on the period of time 1980-
437 2004

438

439 Thirdly, the mean value over the whole set of data was calculated obtaining T_{Lm2}=3.39. The three
440 different statistical averages of T_{Lm2}, i.e., mean daily values, monthly mean hourly values and a
441 constant value of 3.39 have been considered as input in the ESRA model and their respective
442 performances tested over a set of data different from that of the calibration process; this will be
443 discussed in the next section.

444

445 *Performance of the calibrated models*

446

447 The performance of equations developed in this section corresponding to calibrated or locally adapted
448 models is next tested. A set of data different from that used in the adaptation process is used. This new
449 data set corresponds to the period of years 2005-2011. Based on the same criteria given in the last
450 paragraph of section III.A, 9095 data were selected as clear-sky days. Firstly, the performance of the
451 equations (21) and (22) for the Louche and Robledo-Soler models is analyzed; secondly, the
452 performance of the ESRA model by considering the three different averages for T_{Lm2} described above
453 is tested; here, these approaches will be denominated ESRA 1 (daily T_{Lm2} calculated from Bourges
454 algorithm), ESRA 2 (monthly mean hourly values of T_{Lm2} presented in Table V) and ESRA 3 (a
455 constant value T_{Lm2}=3.39)

This manuscript was accepted by Renewable Sustainable Energy. Click here to see the version of record.

Estimated direct horizontal irradiances from the locally adapted models are compared to measured direct horizontal irradiance in Figure 7. Table VI gives the number of data and mean values for each solar altitude angle range corresponding to the period 2005-2011. In Table VII, the statistical errors MBE and RMSE are given for this validation data set.

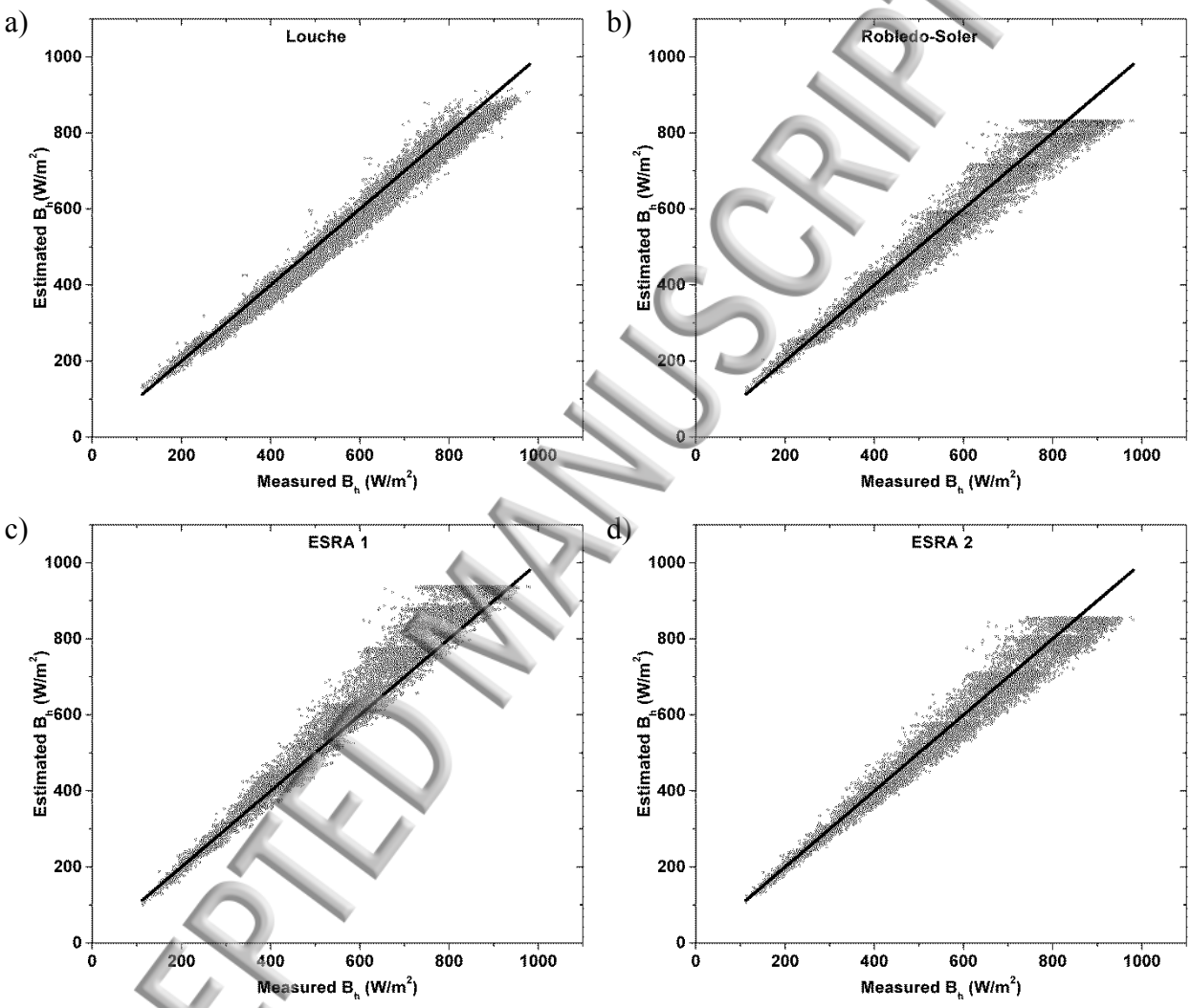

This manuscript was accepted by Renewable Sustainable Energy. Click here to see the version of record.

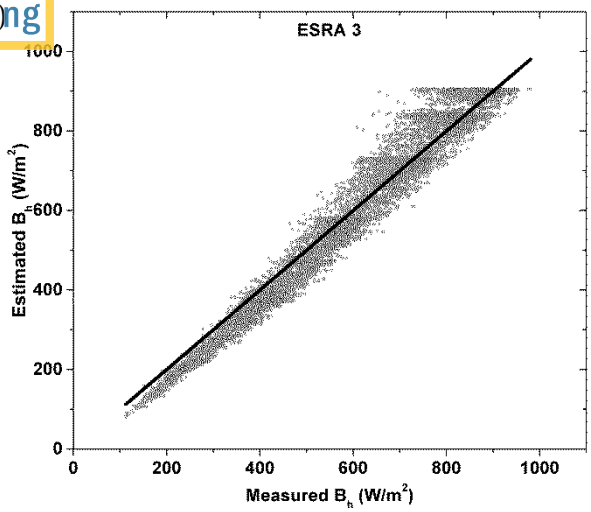

Figure 7. Estimated values of clear-sky direct horizontal irradiance against the corresponding measured values for Louche, Robledo-Soler and ESRA locally adapted models. The time period for this performance analysis is 2005-2011. Solid black line represents the 1:1relationship.

Table VI. Number of data (N) and mean direct horizontal irradiance from measured data at Madrid for different solar altitude angle ranges and for the total data for the period 2005-2011.

α	<20º	20º-40º	40º-60º	>60º	Total
N	656	3334	3185	1920	9095
Mean B_h (W/m^2)	219.68	430.22	666.96	827.96	581.9

Table VII. Performance of the calibrated models (section IV) for different solar altitude angle ranges and for the total data based on the time period 2005-2011.

		MBE(%)					RMSE(%)				
Model	α	<20º	20º-40º	40º-60º	>60º	Total	<20º	20º-40º	40º-60º	>60º	Total
Louche		0.42	-4.93	-2.86	-2.42	-3.2	7.96	7.18	5.08	4.74	5.7
Robledo-Soler		2.4	-2.92	-1.73	-3.3	-2.41	7.44	7.69	6.74	7.02	7.37
ESRA 1		-2.03	2.08	6.79	7.75	5.56	5.81	6.7	9.25	9.9	9.52

ESRA 2	-1.12	-1.72	-1.85	-2.2	-1.9	5.12	6.23	6.34	6.59	6.72
ESRA 3	-16.09	-7.8	0.15	3.35	-1.48	17	10.01	6.33	7.05	7.92

From Table VII, it can be seen that the improvement of the accuracy of models was quite significant; the errors diminished with respect to Table IV. Louche, Robledo-Soler and ESRA 2 models perform better than the rest; specifically, total RMSE was reduced from 9.9% to 5.7%, 7.8 to 7.4% and 8.8 to 6.7%, respectively. Regarding to the three approaches considered for T_{Lm2}, ESRA 2 approach, which considers climatic month-hour values of the Linke factor, gives better estimations than the other two; this is due to ESRA 2 approach considers the significant diurnal variation of the atmospheric turbidity [48] which is larger than the day to day variation (considered in ESRA 1); its MBE and RMSE present similar low values for all the solar altitude angle ranges (MBE=-1.9% and RMSE=6.7% for all data). ESRA 1, which makes use of the Bourges algorithm, also had similar errors for all solar altitude angle ranges (MBE=5.6% and RMSE=9.5% for all data). In the case of ESRA 3, which assume a constant value for T_{Lm2}, the total errors are low (MBE=-1.5% and RMSE=7.9% for all data) but high values are found for the range of low solar altitude angles.

The results shown in this section lead to the conclusion that significant improvements can be obtained when applying solar irradiance parametric models adapted to a specific local area. RMSE values diminish around 4% in Louche model and 2% in the ESRA model. In the case of Robledo-Soler model, this value only decrease 0.4% due to their model was originally established for Madrid; calibrated and original coefficients are close which indicates the accurate determination of the original parametric coefficients. The best performance is attributed to Louche model followed by ESRA 2 and Robledo-Soler, with RMSE values of 5.7%, 6.7% and 7.4% respectively.

V. Conclusions

Radiation modelling is an important factor in the design of renewable solar power systems. Accurate prediction of the direct component of solar irradiance is essential in applications which require high-concentration radiation intensity. To evaluate the performance of solar radiation models, availability of direct irradiance based on long-term experimental data is essential. In the first part of this work, eight well-referenced models were analyzed in order to calculate direct horizontal irradiance under

This manuscript was accepted by Renewable Sustainable Energy. Click here to see the version of record.

clear skies by using experimental data taken in Madrid, Spain, on a hourly basis. The period of time from 1980 to 2004 has been considered for this analysis. Three models with the best performance were selected in the next step in order to quantify the improvement in the modelled values by fine-tuning them to local conditions. Calibrated algorithms for Madrid are given by the equations (21) and (22) for the Louche and Robledo-Soler models. In the case of ESRA model, three different approaches, regarding to the Linke factor (T_{Lm2}) input values, are considered. Calibrated (locally adapted) models were validated against a different set of data corresponding to years 2005-2011. Low performance errors are obtained in general as it is shown in Table VII. When compared with the RMSE in Table IV, it can be seen how they have decreased from 9.9 % to 5.7%, 7.8% to 7.4% and 8.8% to 6.7% for the models of Louche, Robledo-Soler and the approach here called ESRA 2, respectively. This means that an improvement up to 4% can be achieved in the direct horizontal irradiance estimations when parametric models are adapted to a specific local site. In the case of Robledo-Soler, it is only a 0.4% due to parametric coefficients were also initially established to Madrid. It is expected that calibrated algorithms presented in this work will be useful to estimate solar direct horizontal irradiance in regions of similar climatic characteristics.

Acknowledgements

This research received economic support from the Spanish Government (grant ENE2011-27511) and the Department of Culture and Education of the Regional Government of Castilla y León, Spain (grant BU358A12-2). The authors wish to thank the National Meteorological Agency in Spain (AEMET) for supplying the data used in this work.

NOMENCLATURE SECTION

B_n	direct normal irradiance (W/m^2)
B_h	direct horizontal irradiance (W/m^2)
D_h	diffuse horizontal irradiance (W/m^2)
G_h	global horizontal irradiance (W/m^2)
E_0	Correction factor for the sun-earth distance

This manuscript was accepted by Renewable Sustainable Energy. Click here to see the version of record.

530	I_0	normal extraterrestrial irradiance (W/m^2)
531	I_{sc}	Solar constant (W/m^2)
532	J	day number of the year
533	K_b	atmospheric direct transmittance
534	K_d	diffuse fraction
535	K_t	clearness index
536	MBE	mean bias error (%)
537	m	relative optical air mass
538	p	pressure (mb)
539	p_0	standard pressure (1013.25 mb)
540	$RMSE$	root mean square error (%)
541	T_{Lm2}	Linke turbidity factor for an air mass equal to 2
542	Γ	day angle (º)
543	z	height of the site above sea level (m)
544	α	solar altitude angle (º)
545	ε	Perez's sky clearness index
546	δ_R	Rayleigh optical depth
547	θ	solar zenith angle (º)

548

549

550 **References**

551

552 [1] Communication from the European Parliament, the Council, the European Economic and

553 Social Committee and the Commettee of the Regions: Energy Roadmap 2050. (COM/2011/0885

554 final), 2011

555 [2] IDAE, National Action Plan for Renewable Energy in Spain (PANER) 2011-2020, 2010

556 [3] N. R. Darghouth, G. Barbose, R. Wiser, The impact of rate design and net metering on the bill

557 savings from distributed PV for residential customers in California, Energy Policy 39(9), 5243-5253

558 (2011)

559 [4] D. González-Peña, M. Díez-Mediavilla, M. de Simón-Martín, M. C. Rodríguez-Amigo, T.
560 García-Calderón, C. Alonso-Tristán, Photovoltaic Prediction Software and Their Evaluation with
561 Real Data in Spain, 27th European Photovoltaic Solar Energy Conference and Exhibition,
562 Frankfurt (Germany), 2012.
563 [5] V. Badescu, C. A. Gueymard, S. Cheval, C. Oprea, M. Baciu, A. Dumitrescu, F. Iacobescu, I.
564 Milos, C. Rada, Accuracy analysis for fifty-four clear-sky solar radiation models using routine
565 hourly global irradiance measurements in Romania, Renewable Energy 5, 585-103 (2013)
566 [6] K. De Souza and R. Andrews, Models for daily global solar radiation for the Caribbean island of
567 Trinidad, J. Renewable Sustainable Energy 7, 013132 (2015)
568 [7] C. A. Gueymard, Direct solar transmittance and irradiance predictions with broadband
569 models. Part I: Detailed theoretical performance assessment, Solar Energy 74, 355-379 (2003)
570 [8] M. Iqbal, An introduction to solar radiation, Academic Press, 1983.
571 [9] C. Rigollier, O. Bauer, L. Wald, on the clear sky model of the ESRA - European Solar
572 Radiation Atlas - With respect to the Heliosat method, Solar Energy 68, 33-48 (2000)
573 [10] A. Hammer, D. Heinemann, C. Hoyer, R. Kuhlemann, E. Lorenz, R. Müller, H. G. Beyer,
574 Solar energy assessment using remote sensing technologies, Remote Sensing of Environment 86,
575 423-432 (2003)
576 [11] C. A. Gueymard, Progress in direct irradiance modeling and validation, 39th ASES National
577 Solar Conference, SOLAR 2010, Phoenix, USA, 2010
578 [12] C. A. Gueymard, Clear-sky irradiance predictions for solar resource mapping and large-scale
579 applications: Improved validation methodology and detailed performance analysis of 18
580 broadband radiative models, Solar Energy 86, 2145-2169 (2012)
581 [13] L. T. Wong, W. K. Chow, Solar radiation model, Applied Energy 69 191-224 (2001)

582 [14] R. Perez, R. Seals, A. Zelenka, P. Ineichen, Climatic evaluation of models that predict
583 hourly direct irradiance from hourly global irradiance: Prospects for performance improvements,
584 Solar Energy 44, 99-108 (1990)
585 [15] F. J. Batlles, M. A. Rubio, J. Tovar, F. J. Olmo, L. Alados-Arboledas, Empirical modeling of
586 hourly direct irradiance by means of hourly global irradiance, Energy 25, 675-688 (2000)
587 [16] J. L. Torres, M. De Blas, A. García, A. de Francisco, Comparative study of various models
588 in estimating hourly diffuse solar irradiance, Renewable Energy 35, 1325-1332 (2010)
589 [17] S. Dervishi, A. Mahdavi, Computing diffuse fraction of global horizontal solar radiation: A
590 model comparison, Solar Energy 86, 1796-1802 (2012)
591 [18] P. J. Pérez-Higueras, P. Rodrigo, E. F. Fernández, F. Almonacid, L. Hontoria, A simplified
592 method for estimating direct normal solar irradiation from global horizontal irradiation useful for
593 CPV applications, Renewable and Sustainable Energy Reviews 16, 5529-5534 (2012)
594 [19] M. Bortolini, M. Gamberi, A. Graziani, R. Manzini, C. Mora, Multi-location model for the
595 estimation of the horizontal daily diffuse fraction of solar radiation in Europe, Energy Conversion
596 and Management 67, 208-216 (2013)
597 [20] H. C. Hottel, A simple model for estimating the transmittance of direct solar radiation
598 through clear atmospheres, Solar Energy 18, 129-134 (1976)
599 [21] L. Robledo, A. Soler, Luminous efficacy of direct solar radiation for clear skies, Energy 25,
600 689-701 (2000)
601 [22] C. Bertrand, G. Vanderveken, M. Journee, Evaluation of decomposition models of various
602 complexity to estimate the direct solar irradiance over Belgium, Renewable Energy 74, 618–626
603 (2015)
604 [23] D. T. Reindl, W. A. Beckman, J. A. Duffie, Diffuse fraction correlations, Solar Energy 45,

605 1-7 (1990).

606 [24] D. G. Erbs, S. A. Klein, J. A. Duffie, Estimation of the diffuse radiation fraction for hourly,
607 daily and monthly-average global radiation, Solar Energy 28, 293-302 (1982)

608 [25] T. Muneer, Gul, M. S., Kambezidis, H. D., Allwinkle, S., An all-sky solar meteorological
609 radiation model for the U.K., Proceedings of the Joint CIBSE/ASHRAE Conference, Harrogate,
610 U.K., 1996.

611 [26] P. Ineichen, Comparison and validation of three global-to-beam irradiance models against
612 ground measurements, Solar Energy 82, 501-512 (2008)

613 [27] T. Muneer, Solar radiation and daylight models, 2nd ed., Elsevier Butterworth-Heinemann,
614 Oxford, U.K., 2004.

615 [28] A. Louche, G. Notton, P. Poggi, G. Simonnot, Correlations for direct normal and global
616 horizontal irradiation on a French Mediterranean site, Solar Energy 46, 261-266 (1991).

617 [29] A.L. Maxwell, A quasi-physical model for converting hourly global horizontal to direct
618 normal insolation. Report SERI/TR-215-3087, Solar Energy Research Institute. Golden, CO.
619 USA, 1987.

620 [30] Centre Energétique et Procédés of Ecole des Mines de Paris, Helioclim: Providing
621 information on solar radiation, available in: http://www.helioclim.org/index.html

622 [31] A. Pérez-Burgos, J. Bilbao and A. de Miguel, An evaluation of illuminance measurements at
623 Valladolid (Spain), Journal of Atmospheric and Solar-Terrestrial Physics 69(8), 939–946 (2007)

624 [32] AEMET publications, 'La radiacion Solar.pdf' available at www.aemet.es/documents

625 [33] J. M. Gordon. Solar Energy: The State of the Art (2001)

626 [34] D. Yang, P. Jirutitijaroen, W.M. Walsh, Hourly solar irradiance time series forecasting using cloud
627 cover index, Solar Energy, 86 (12), 3531–3543 (2012)

628 [35] J. Robledo, A. Soler, Modeling the luminous efficacy of diffuse solar radiation on inclined
629 surfaces for all sky conditions, Energy Conversion and Management 44, 177-189 (2003)
630 [36]M.S.Gul and T. Muneer, Models for obtaining solar radiation from other meteorological data, Solar
631 Energy 64, 99–108 (1998)
632 [37]C. Yousif, G. Oña and J. Bilbao Santos, Comparison of solar radiation in Marsaxlokk, Malta and
633 Valladolid, Spain, Renewable Energy, 49, 203–206 (2013)
634 [38]C. A. Gueymard and J.A. Ruiz-Arias, Extensive worldwide validation and climate sensitivity
635 analysis of direct irradiance predictions from 1-min global irradiance, Solar Energy , 128, 1-30 (2016)
636 [39] J. Polo, L. F. Zarzalejo, L. Martín, A. A. Navarro, R. Marchante, Estimation of daily Linke
637 turbidity factor by using global irradiance measurements at solar noon, Solar Energy 83,
638 1177-1185(2009)
639 [40] J. Polo, L. F. Zarzalejo, M. Cony, A. A. Navarro, R. Marchante, L. Martín, M. Romero,
640 Solar radiation estimations over India using Meteosat satellite images, Solar Energy 85,
641 2395-2406 (2011)
642 [41] C. A. Gueymard, S. M. Wilcox, Assessment of spatial and temporal variability in the US
643 solar resource from radiometric measurements and predictions from models using ground-based
644 or satellite data, Solar Energy 85, 1068-1084 (2011)
645 [42] F. Kasten, Discussion on the relative optical air mass, Lighting research & technology 25,
646 129-130 (1993)
647 [43] J. Remund, L. Wald, M. Lefevre, T. Ranchin, J. Page, Worldwide Linke turbidity
648 information, Proceedings of ISES Solar World Congress, Goteborg, Sweden, 2003.
649 [44] G. López, C. A. Gueymard, Clear-sky solar luminous efficacy determination using artificial
650 neural networks, Solar Energy 81, 929-939 (2007).

650 [45] B. Bourges, Yearly variations of the Linke turbidity factor. Climatic data handbook of
652 Europe Dordrecht: Kluwer Academic Publishing, 1992.

653 [46] P. Oteiza and A. Pérez Burgos, Diffuse illuminance availability on horizontal and vertical surfaces
654 at Madrid, Spain, Energy Conversion and Management 64, 313-319 (2012)

655 [47] A. Pérez-Burgos, R. Román, J. Bilbao, A. de Miguel, P. Oteiza, Reconstruction of long-term direct
656 solar irradiance data series using a model based on the Cloud Modification Factor, Renewable Energy
657 77, 115–124 (2015)

658 [48] J. Bilbao, R. Román, A. de Miguel, Turbidity coefficients from normal direct solar irradiance in
659 Central Spain, Atmospheric Research 143, 73-84 (2014)

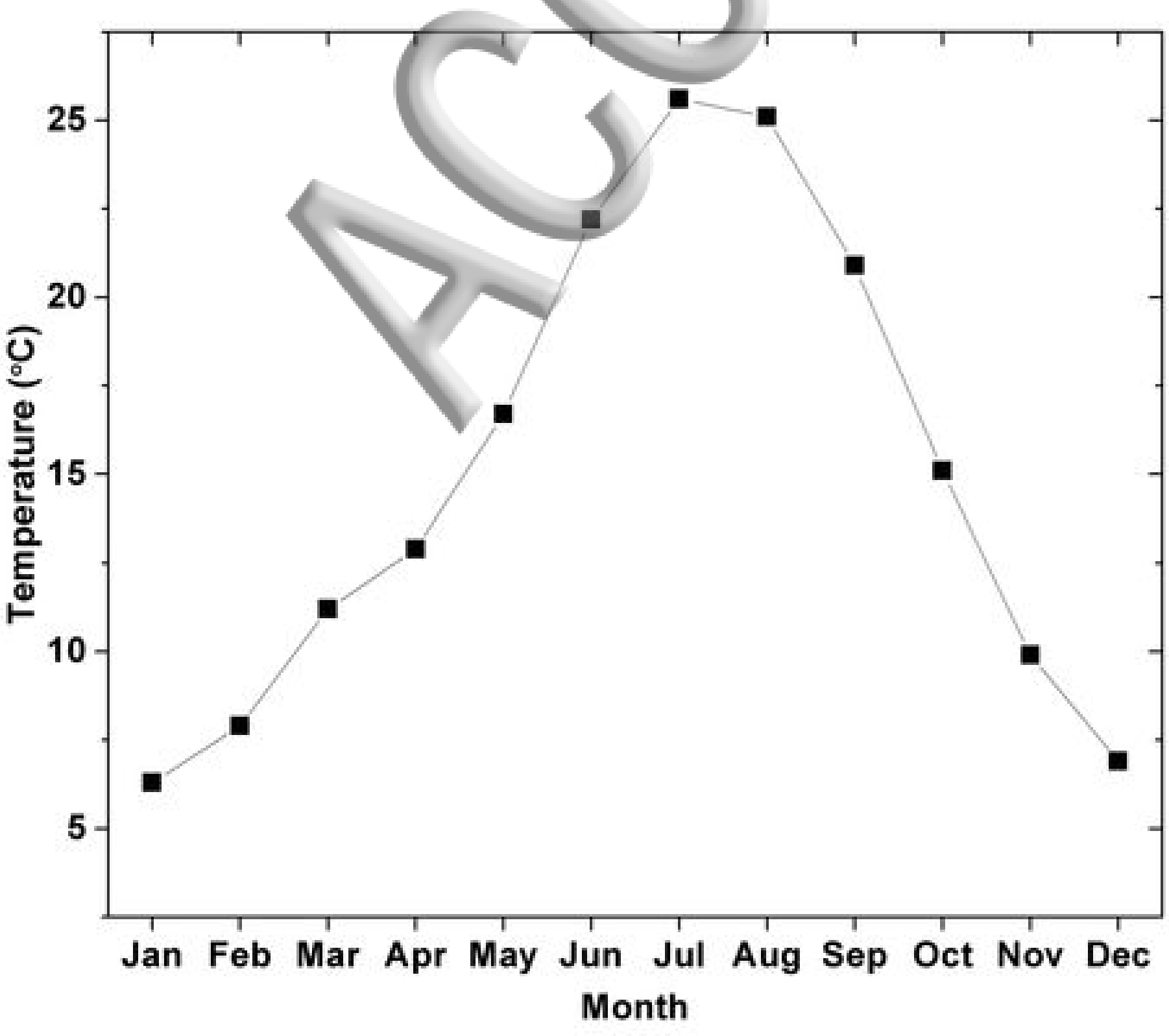
25
20
15
10
5
Temperature (°C)
Jan
Feb
Mar
Apr
May
Jun
Jul
Aug
Sep
Oct
Nov
Dec
Month

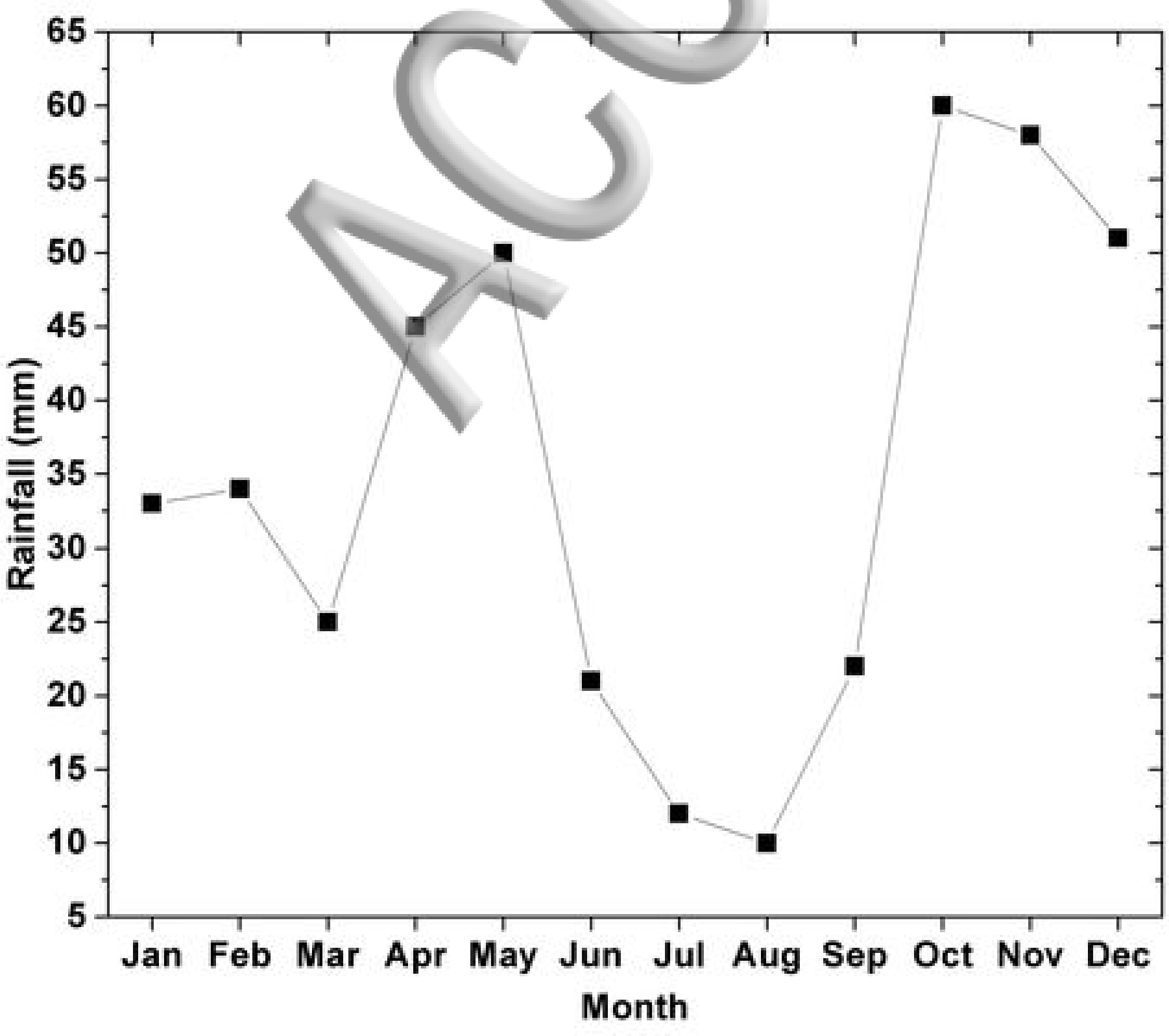
Rainfall (mm)
65
60
55
50
45
40
35
30
25
20
15
10
5
Jan
Feb
Mar
Apr
May
Jun
Jul
Aug
Sep
Oct
Nov
Dec
Month

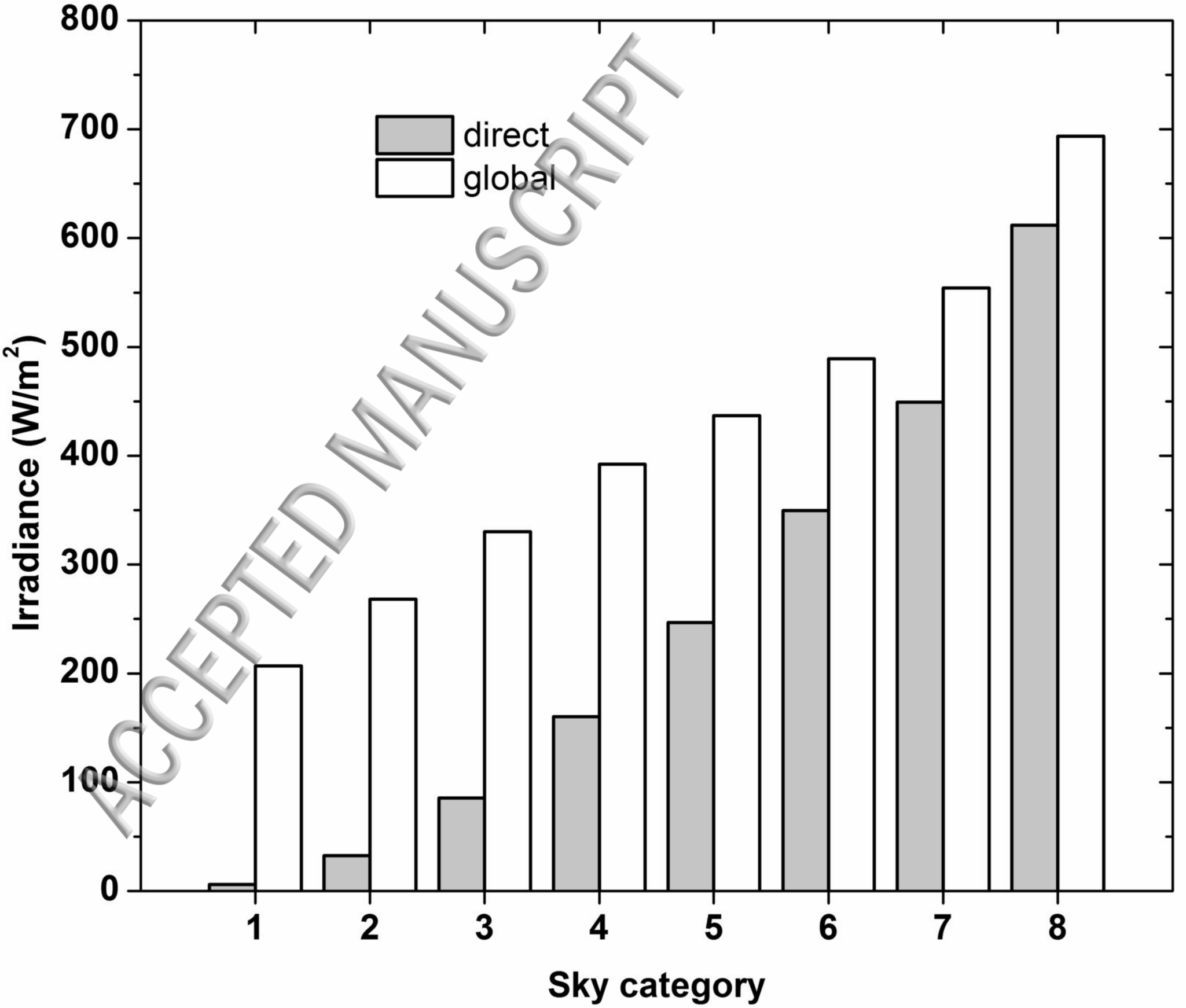

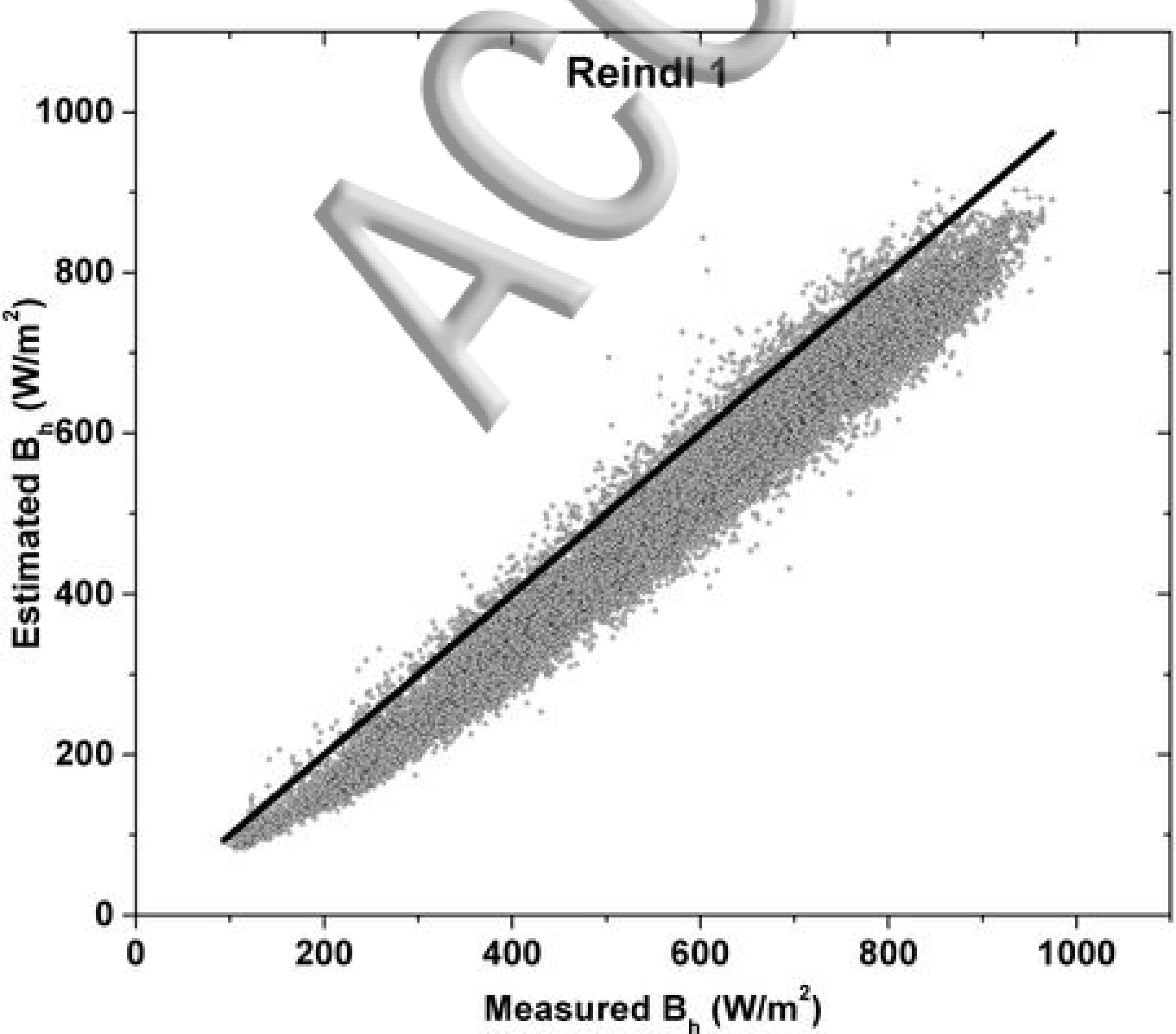
Reindl 1
1000
800
600
400
200
0
0
200
400
600
800
1000
Estimated B_h (W/m^2)
Measured B_h (W/m^2)

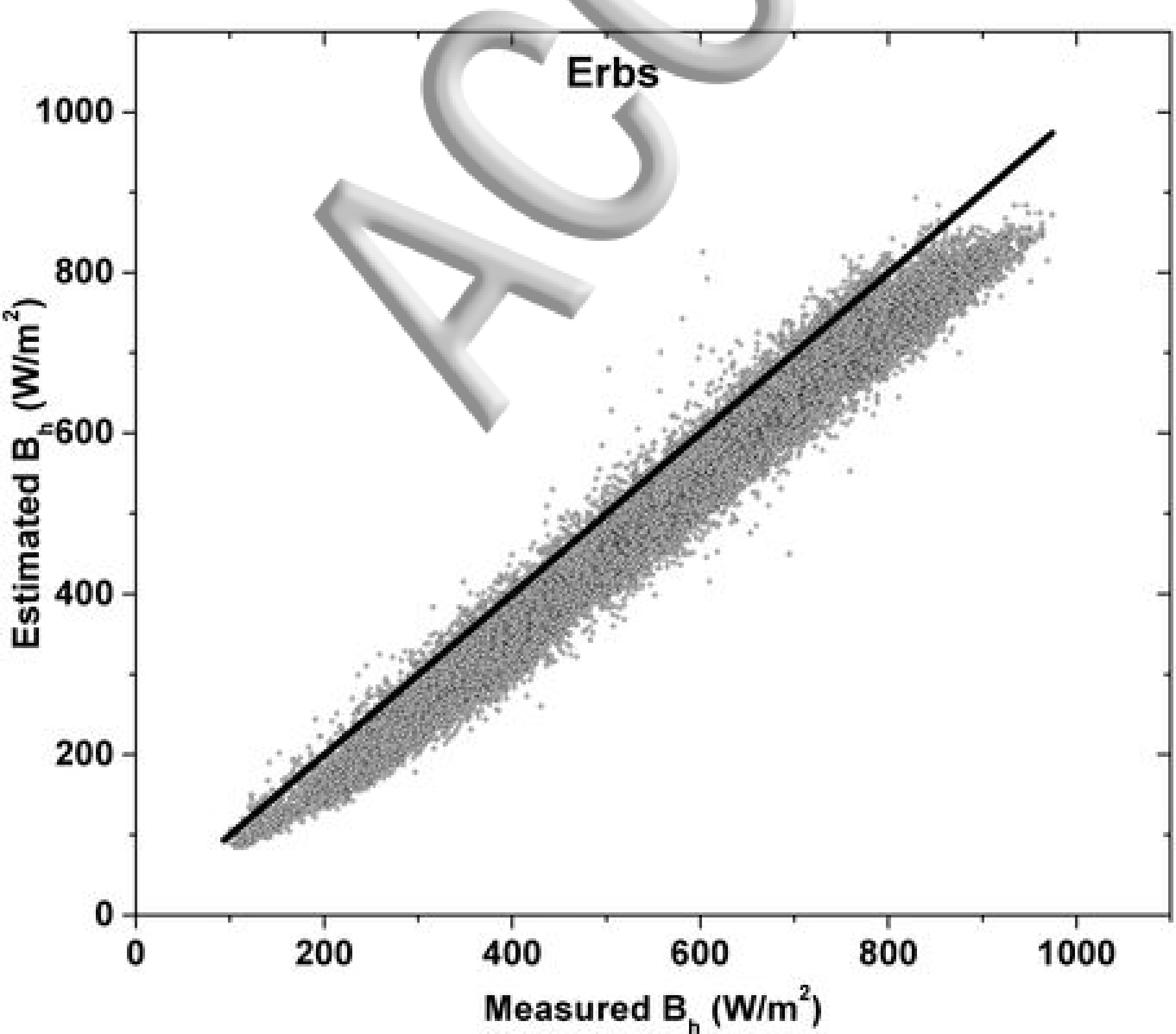
Erbs
1000
800
600
400
200
0
Estimated B_h (W/m^2)
0
200
400
600
800
1000
Measured B_h (W/m^2)

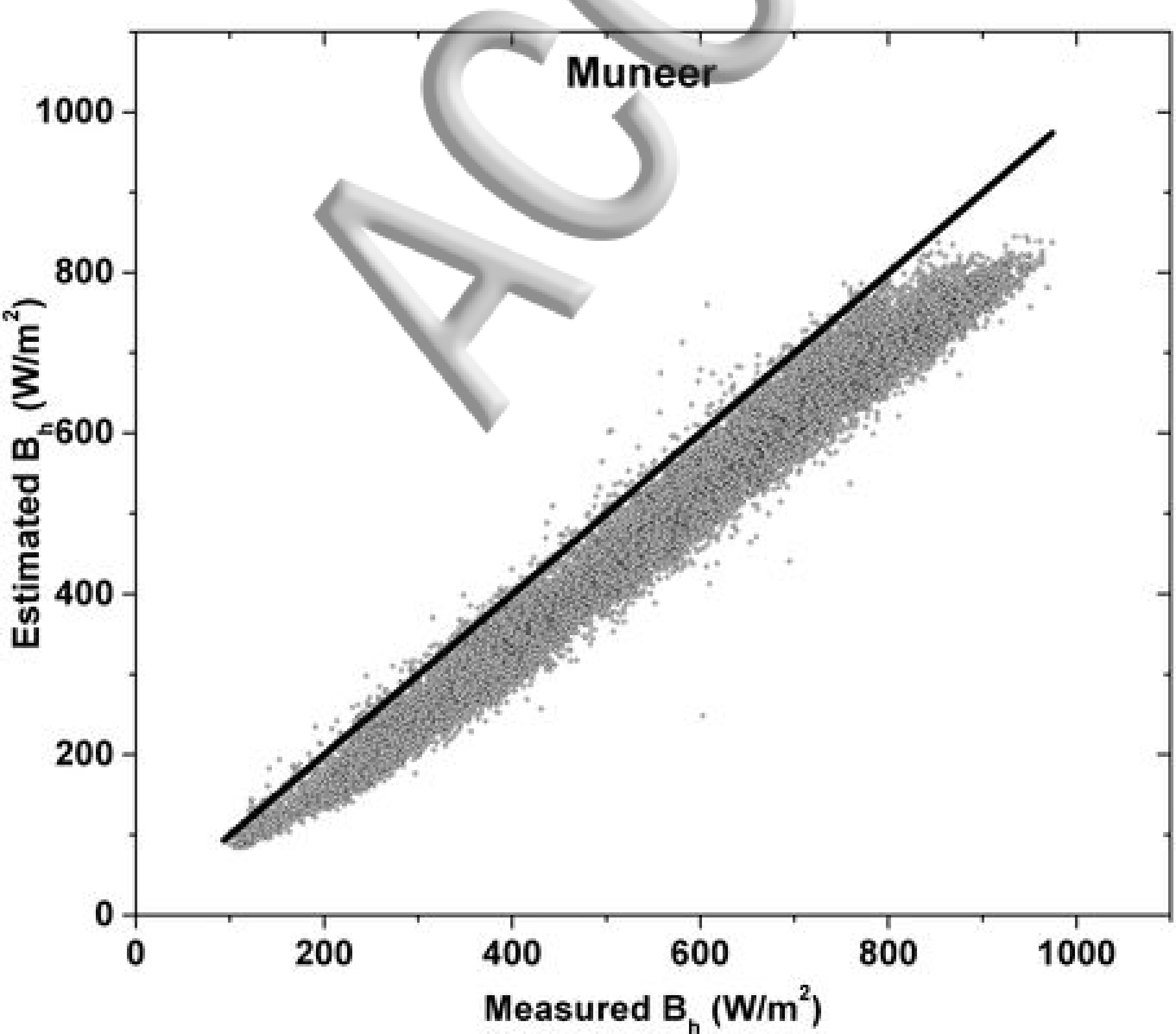
Muneer
1000
800
600
400
200
0
0
200
400
600
800
1000
Estimated B_h (W/m^2)
Measured B_h (W/m^2)

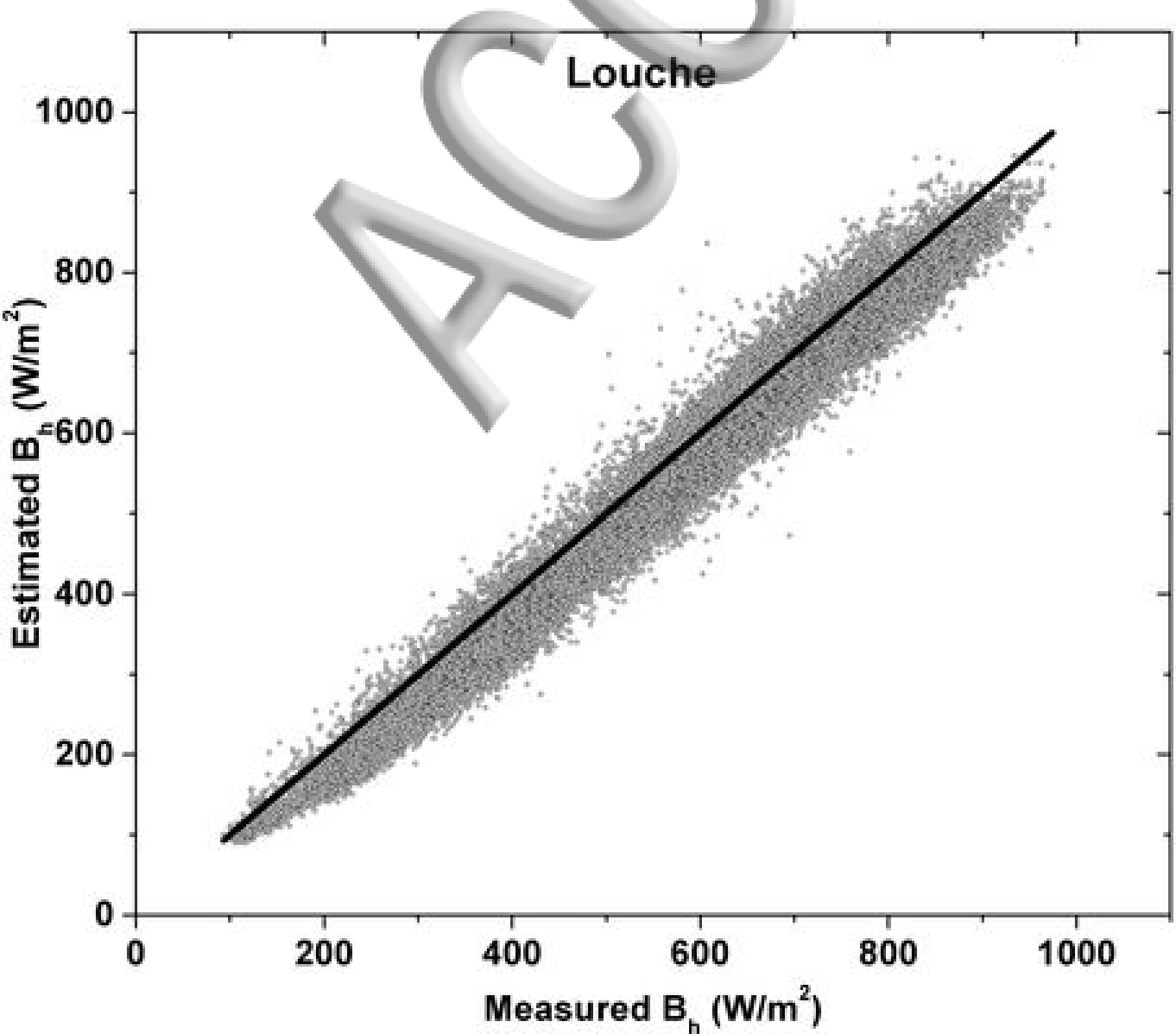
Louche
1000
800
600
400
200
0
0
200
400
600
800
1000
Estimated B_h (W/m^2)
Measured B_h (W/m^2)

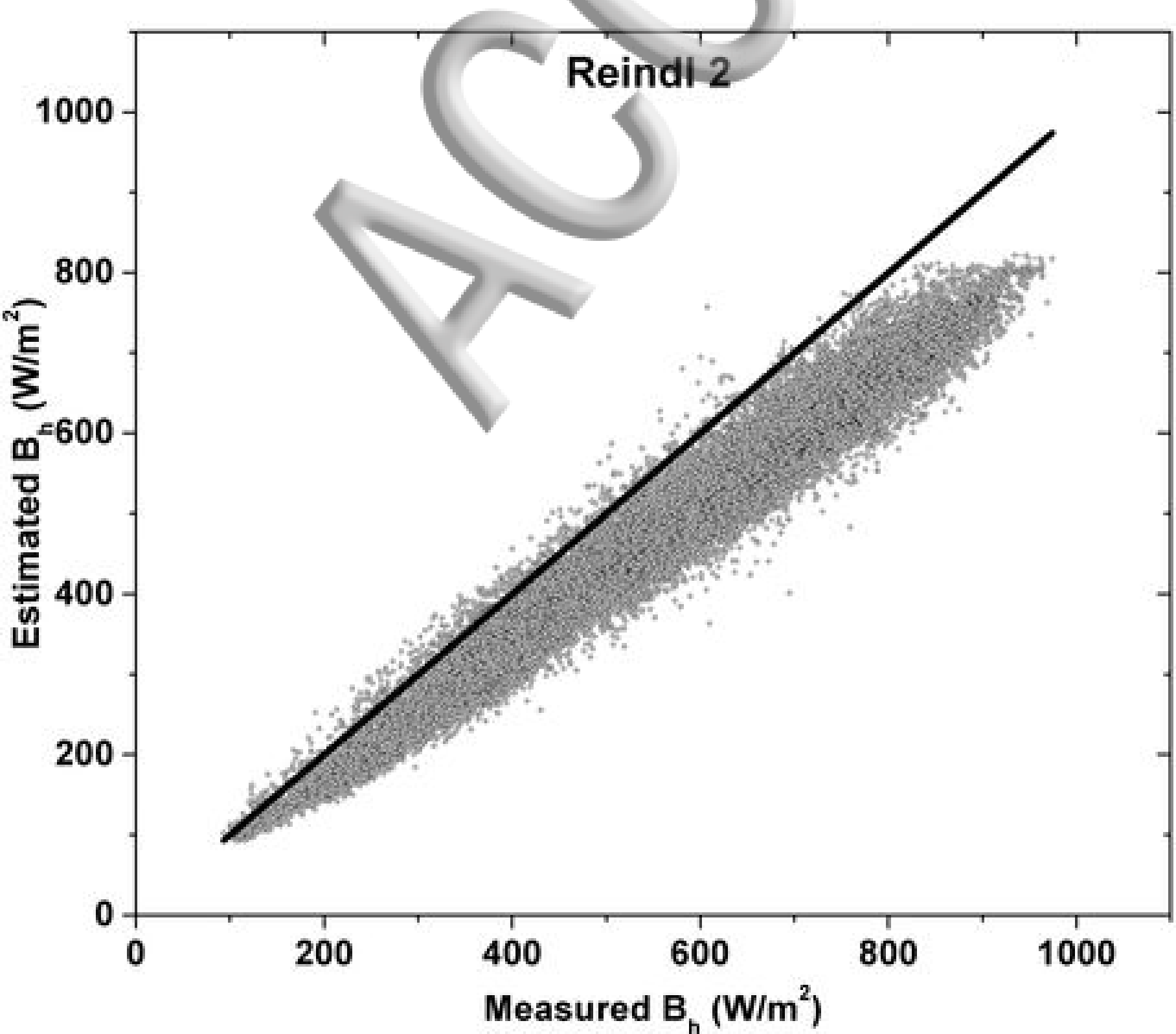
Reindl 2
1000
800
600
400
200
0
Estimated B_h (W/m^2)
0
200
400
600
800
1000
Measured B_h (W/m^2)

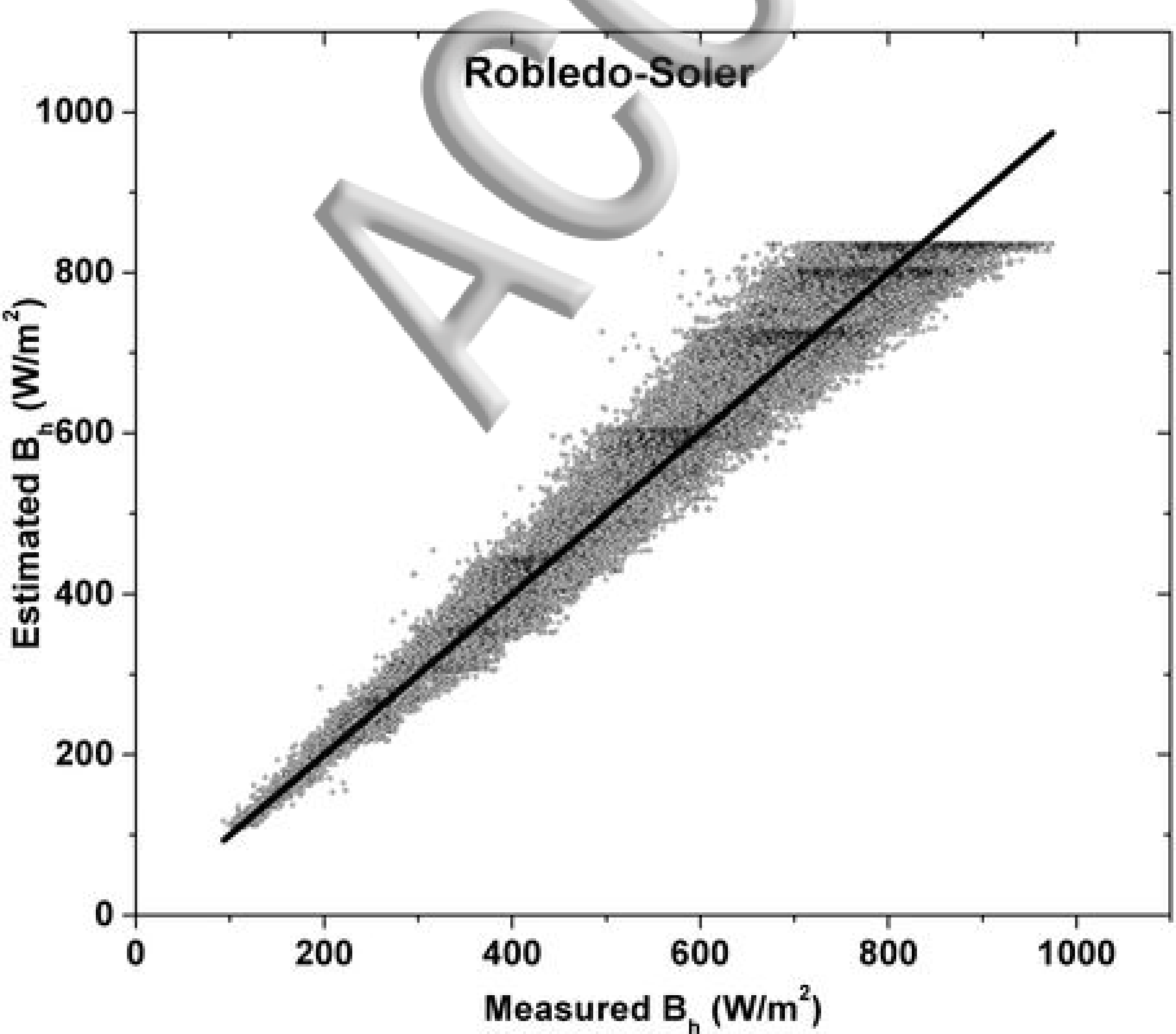
Robledo-Soler
1000
800
600
400
200
0
0
200
400
600
800
1000
Estimated B_h (W/m^2)
Measured B_h (W/m^2)

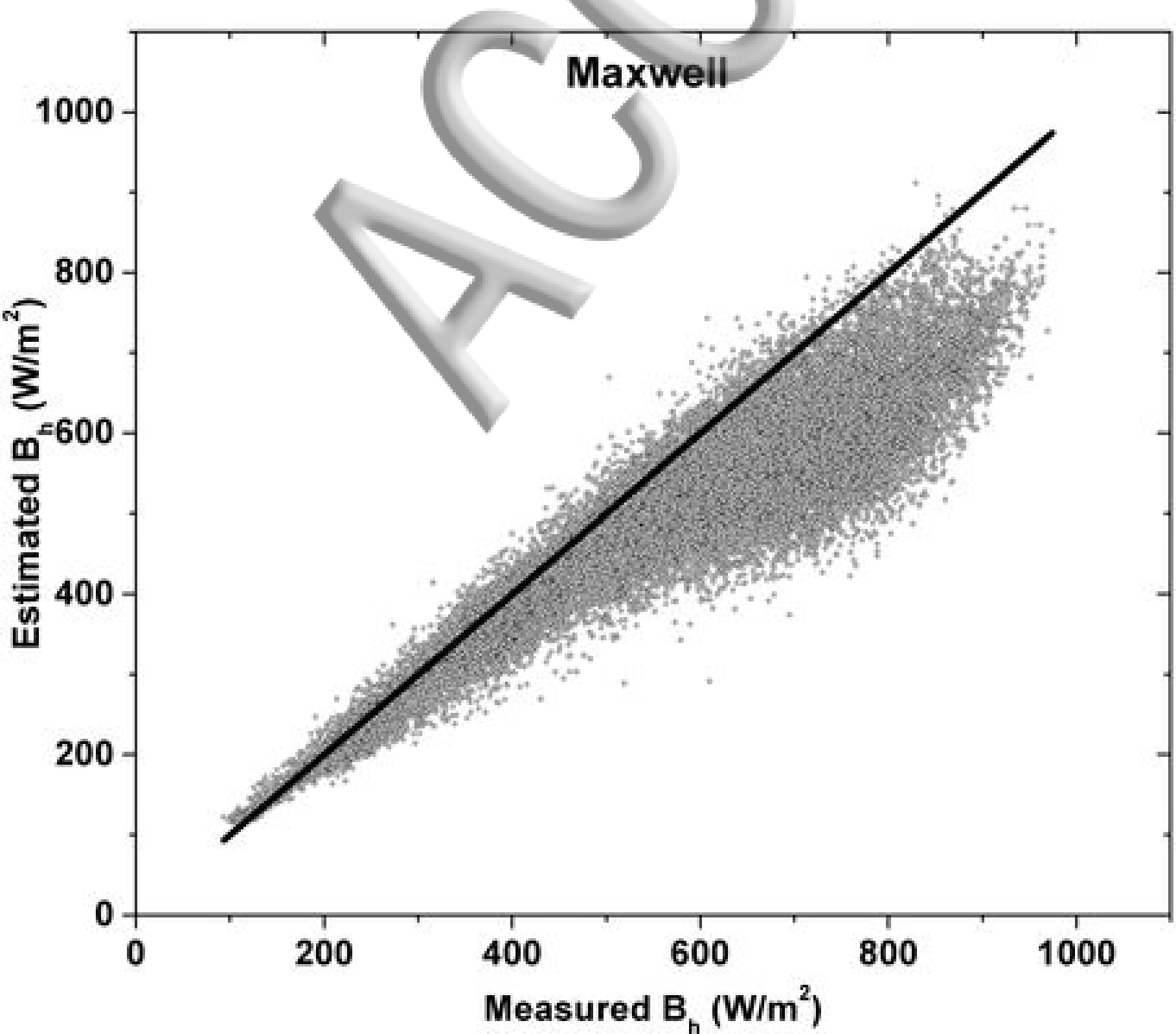
Maxwell
1000
800
600
400
200
0
Estimated B_h (W/m^2)
0
200
400
600
800
1000
Measured B_h (W/m^2)

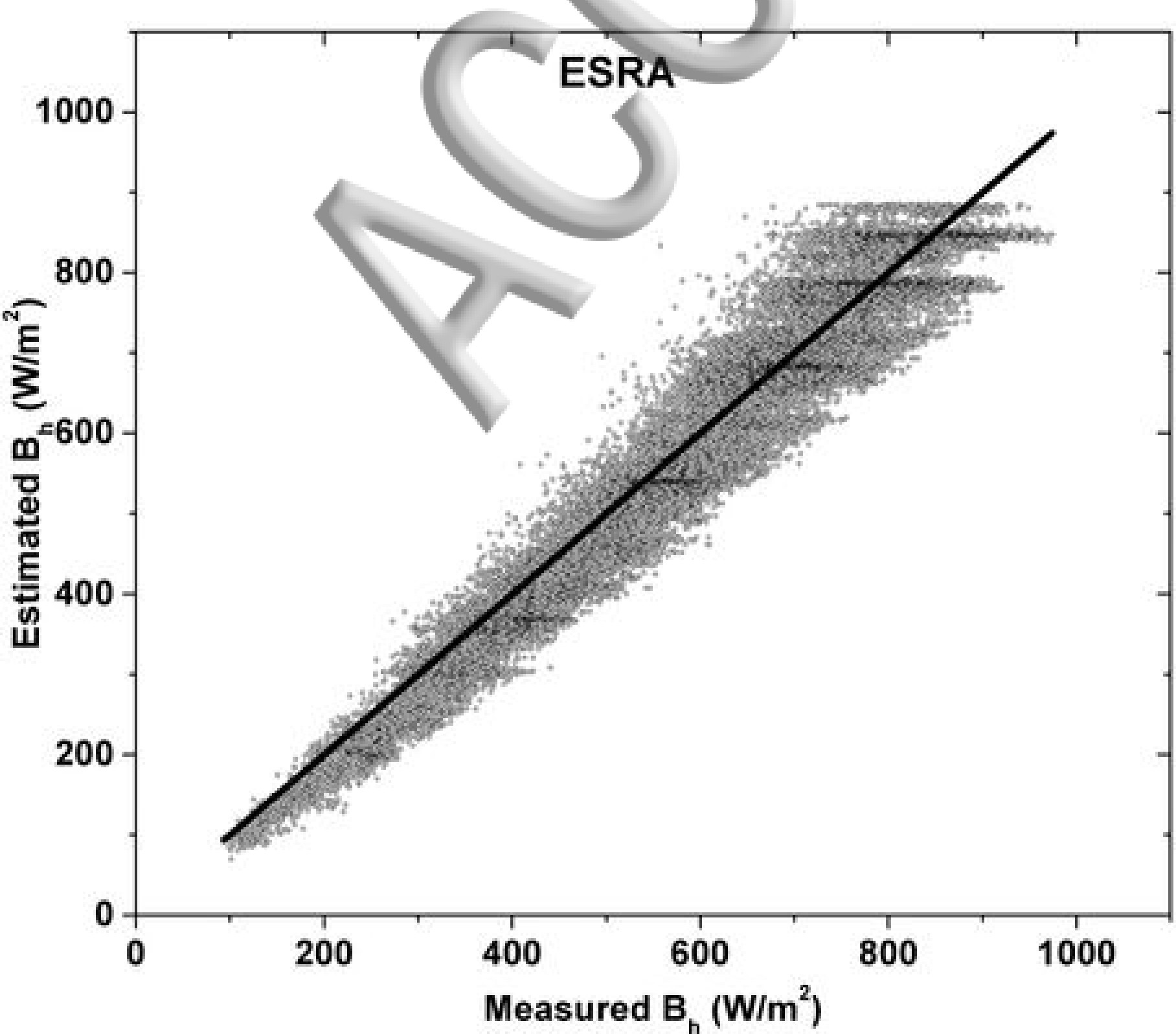
ESRA
1000
800
600
400
200
0
Estimated B_h (W/m^2)
0
200
400
600
800
1000
Measured B_h (W/m^2)

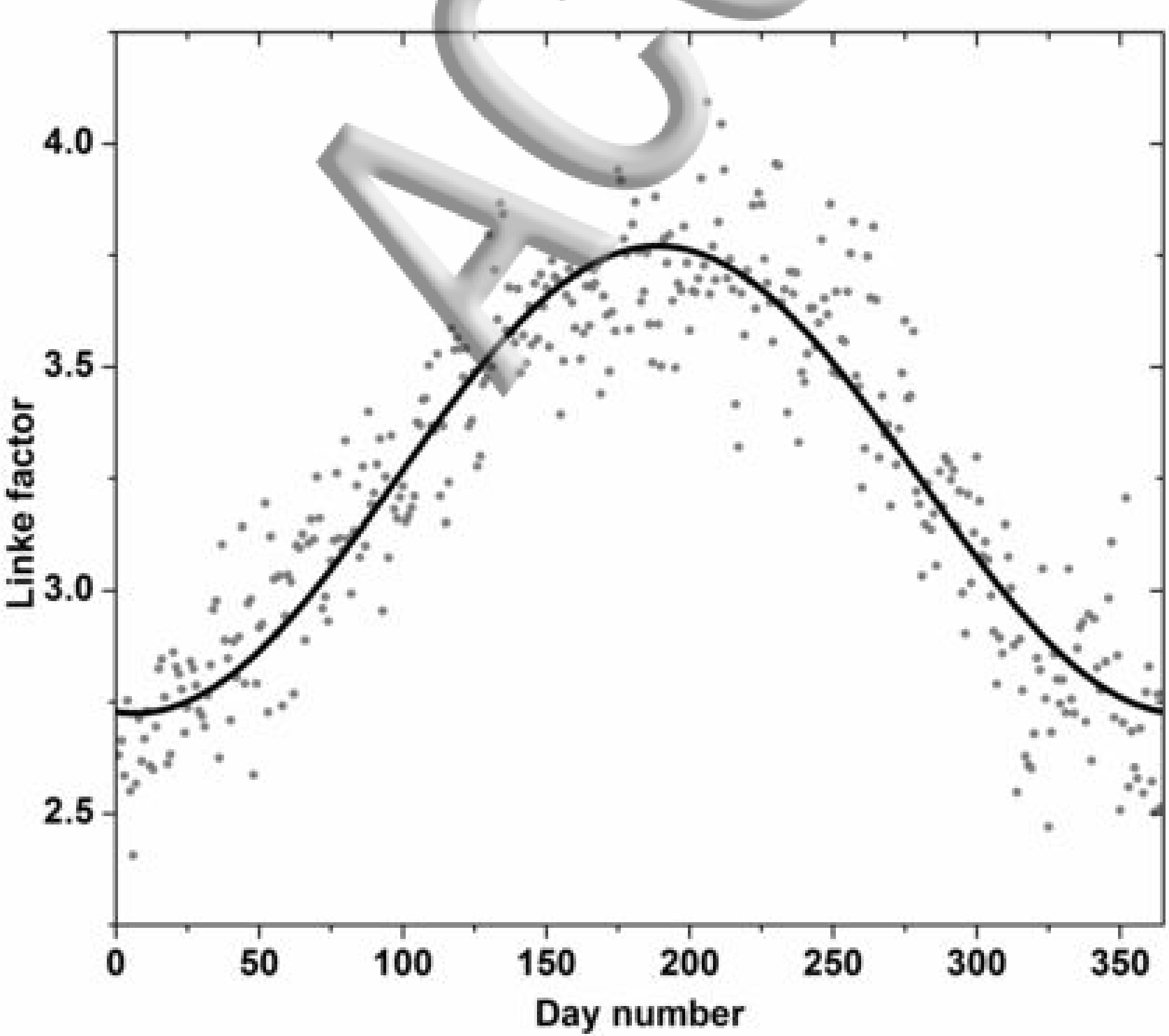
Linke factor
4.0
3.5
3.0
2.5
0
50
100
150
200
250
300
350
Day number

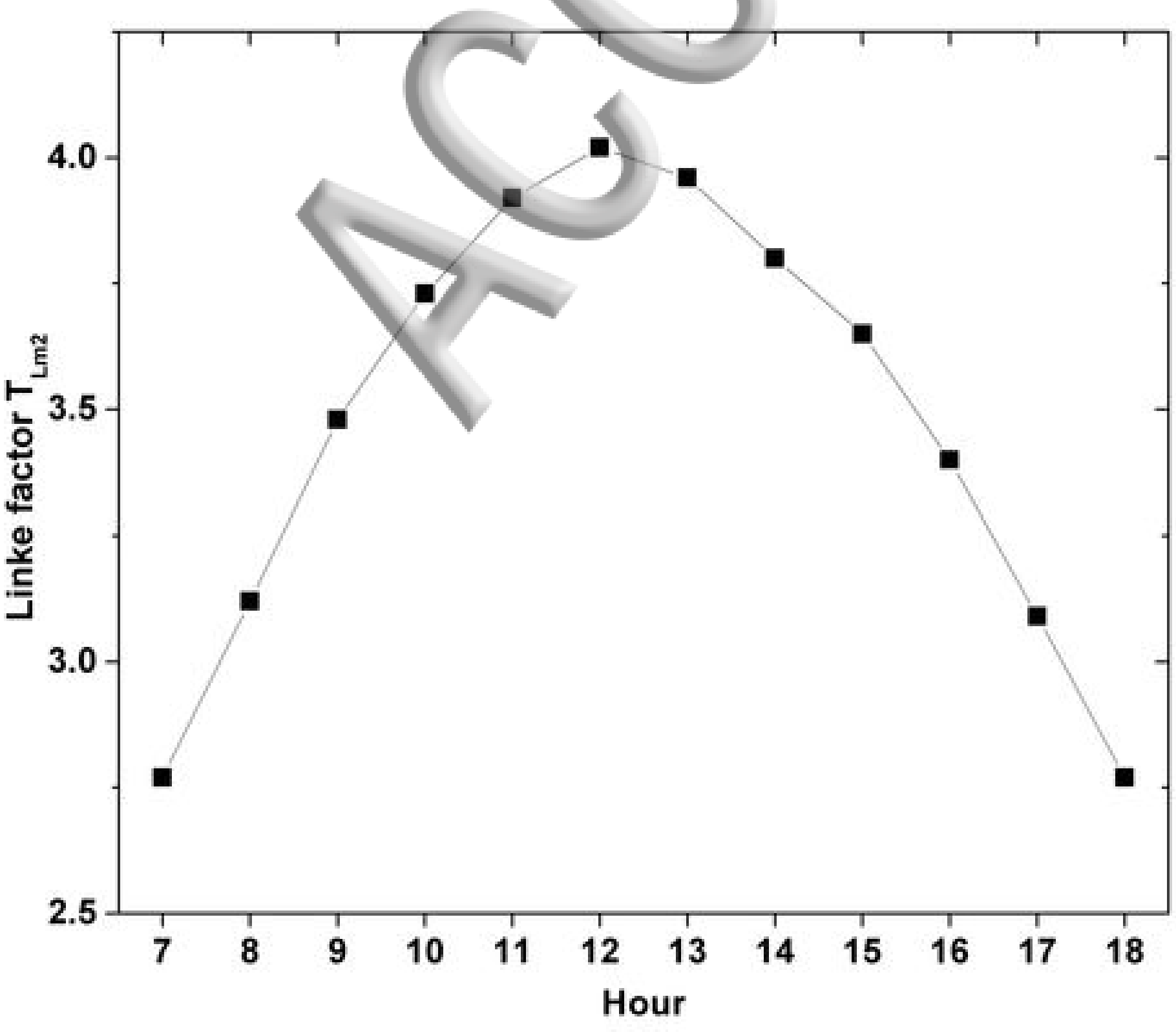
Linke factor T_{Lm2}
4.0
3.5
3.0
2.5
7
8
9
10
11
12
13
14
15
16
17
18
Hour

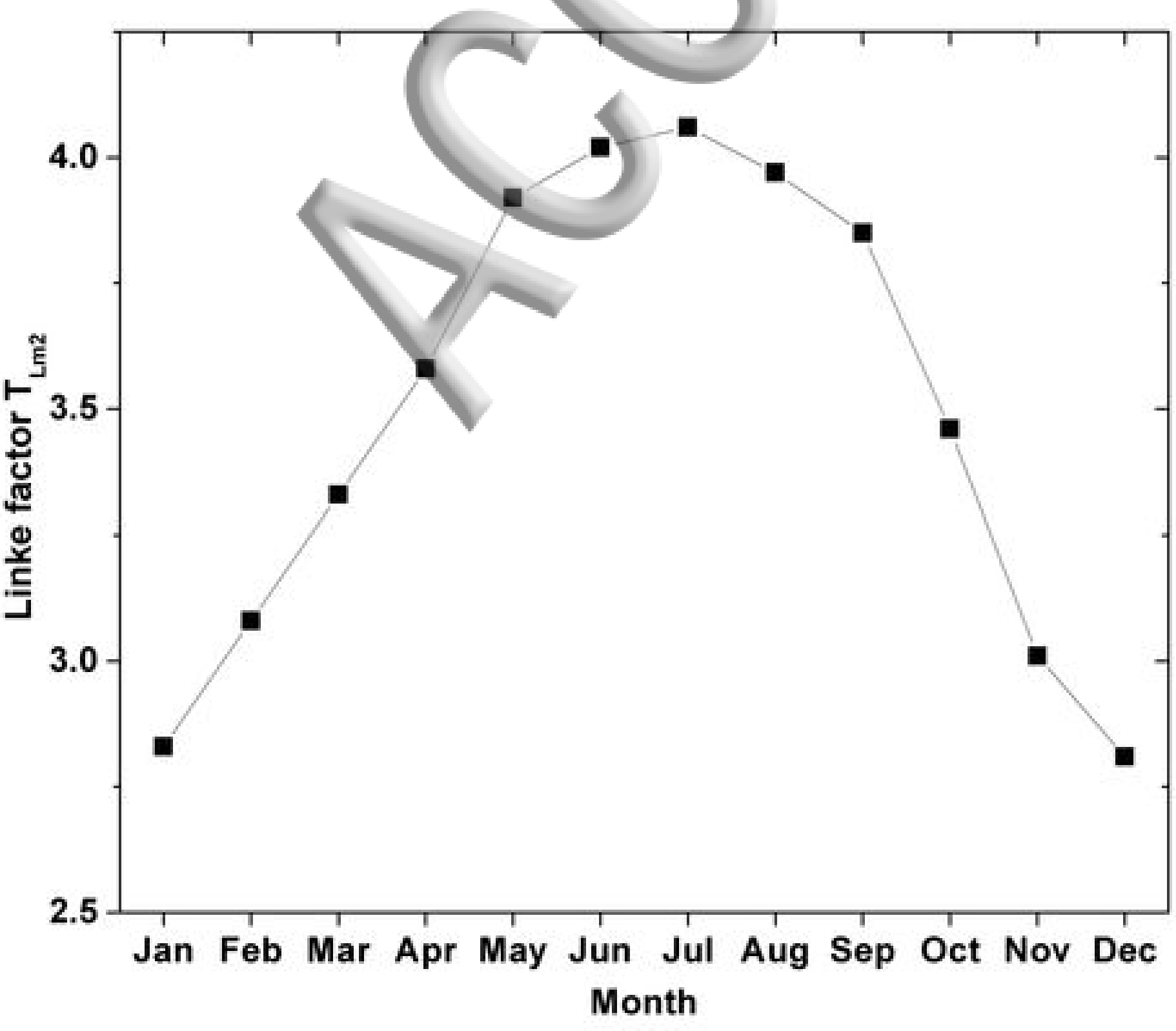
Linke factor T_{Lm2}
4.0
3.5
3.0
2.5
Jan
Feb
Mar
Apr
May
Jun
Jul
Aug
Sep
Oct
Nov
Dec
Month

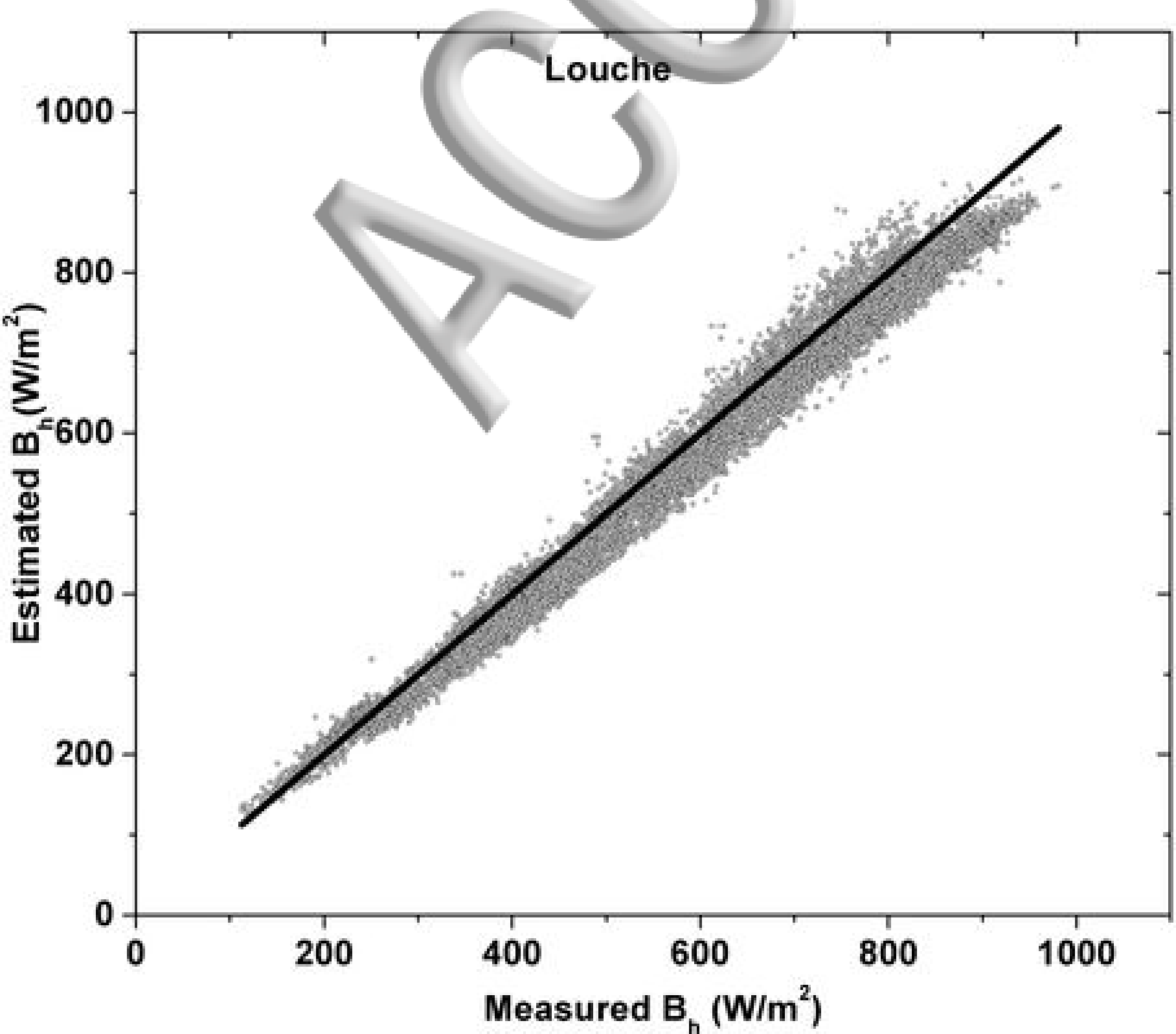
Louche
1000
800
600
400
200
0
0
200
400
600
800
1000
Estimated B_h (W/m^2)
Measured B_h (W/m^2)

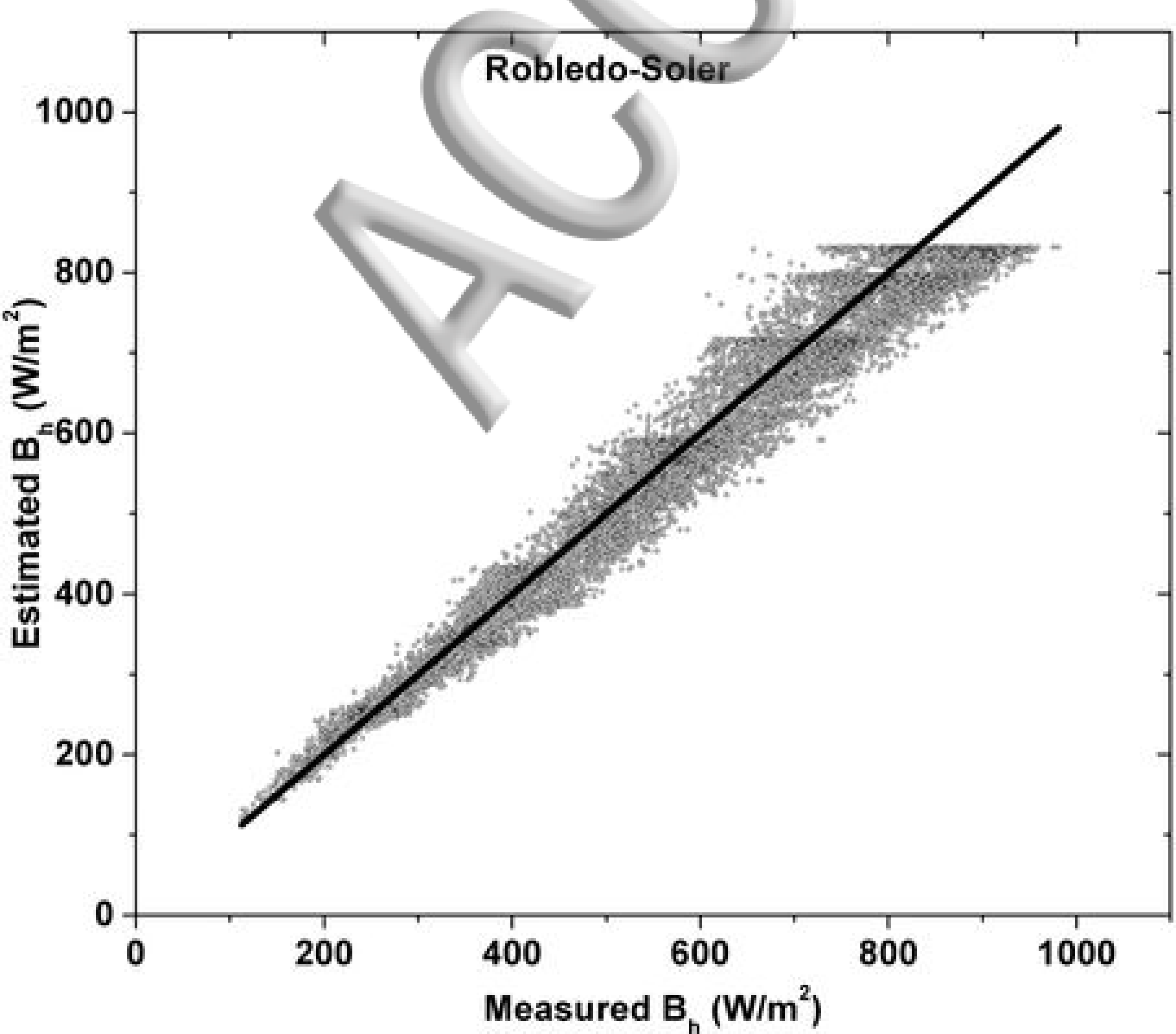
Robledo-Soler
1000
800
600
400
200
0
0
200
400
600
800
1000
Estimated B_h (W/m^2)
Measured B_h (W/m^2)

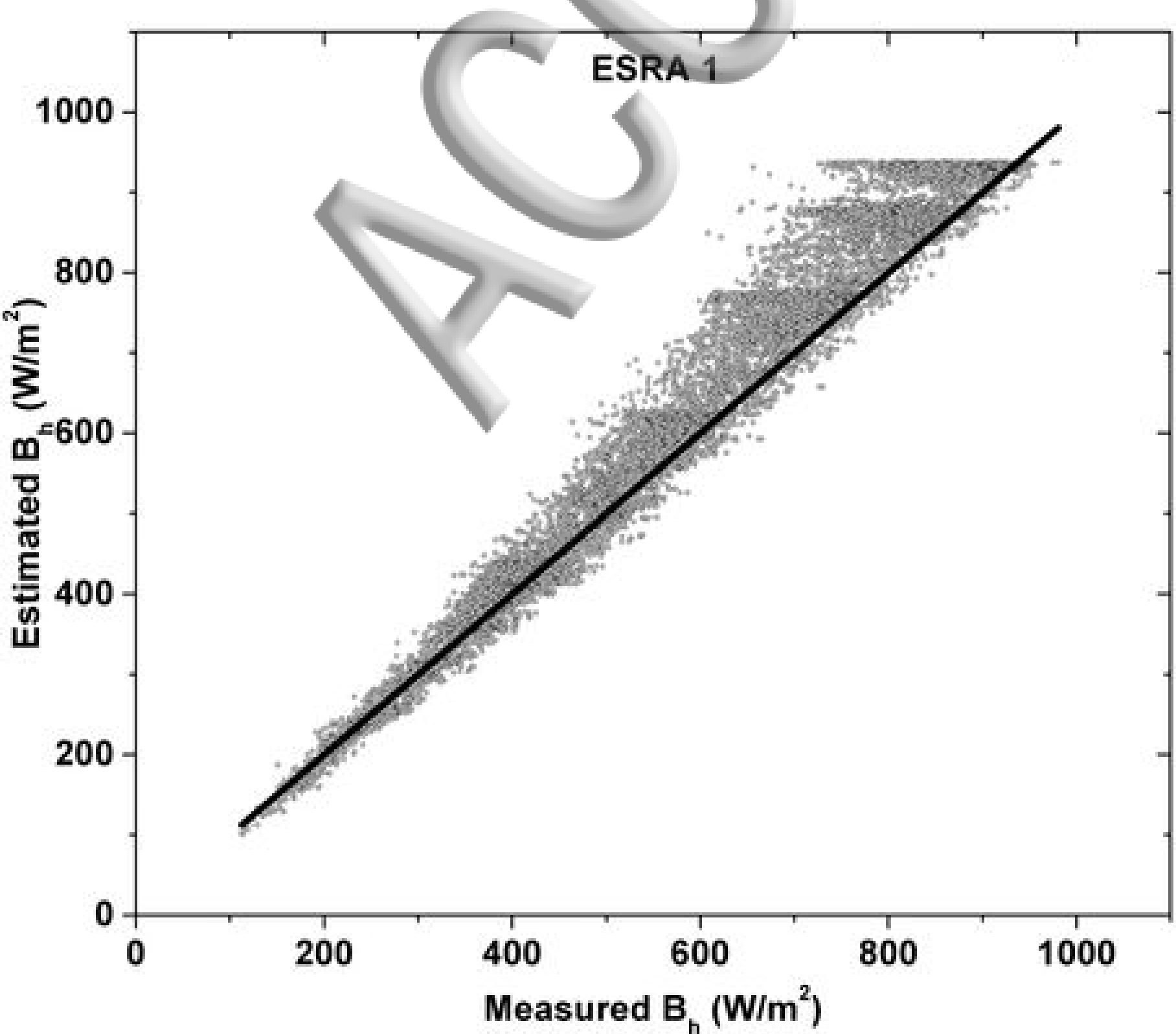
ESRA 1
1000
800
600
400
200
0
0
200
400
600
800
1000
Estimated B_h (W/m^2)
Measured B_h (W/m^2)

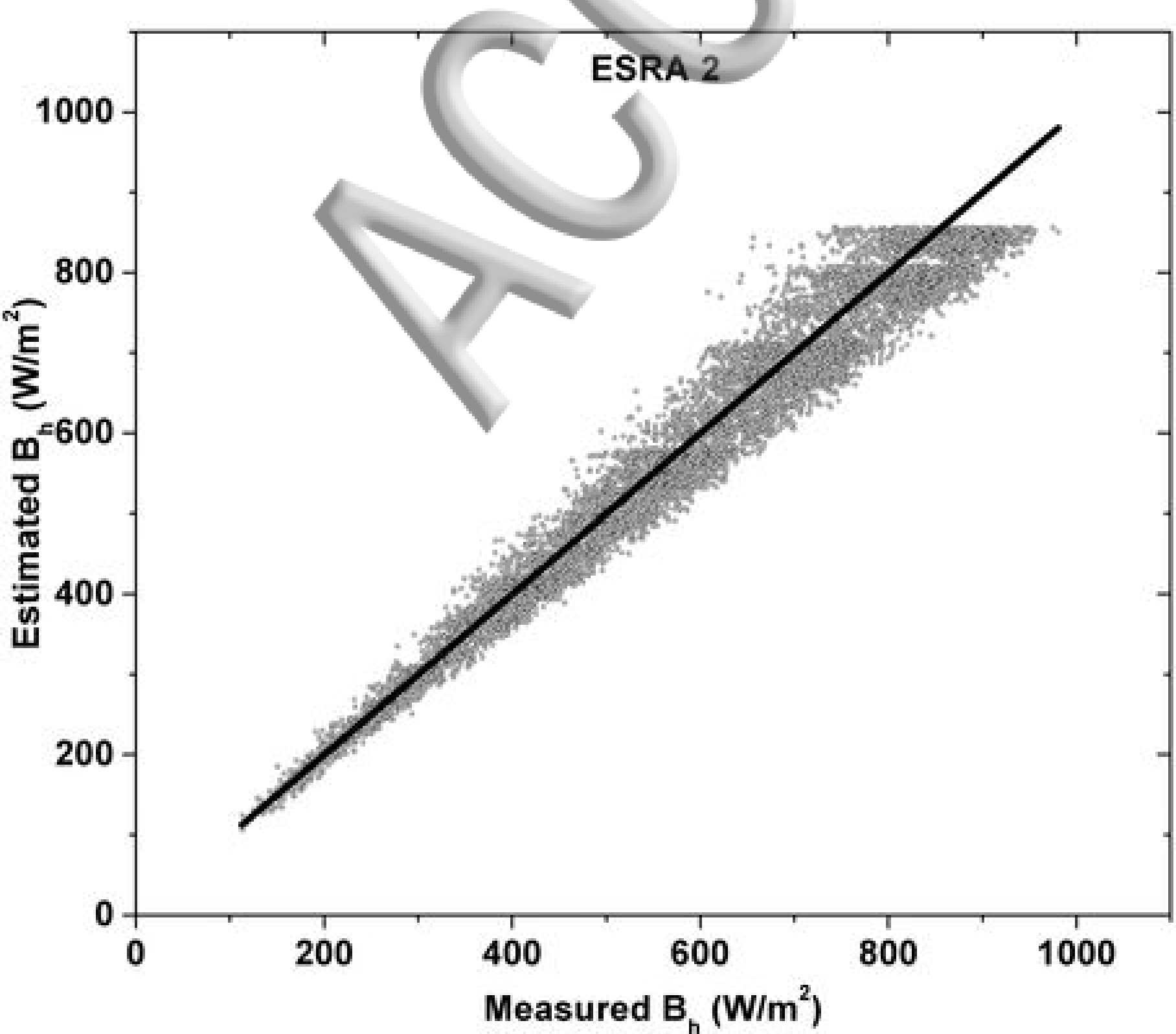
ESRA 2
1000
800
600
400
200
0
Estimated B_h (W/m^2)
0
200
400
600
800
1000
Measured B_h (W/m^2)

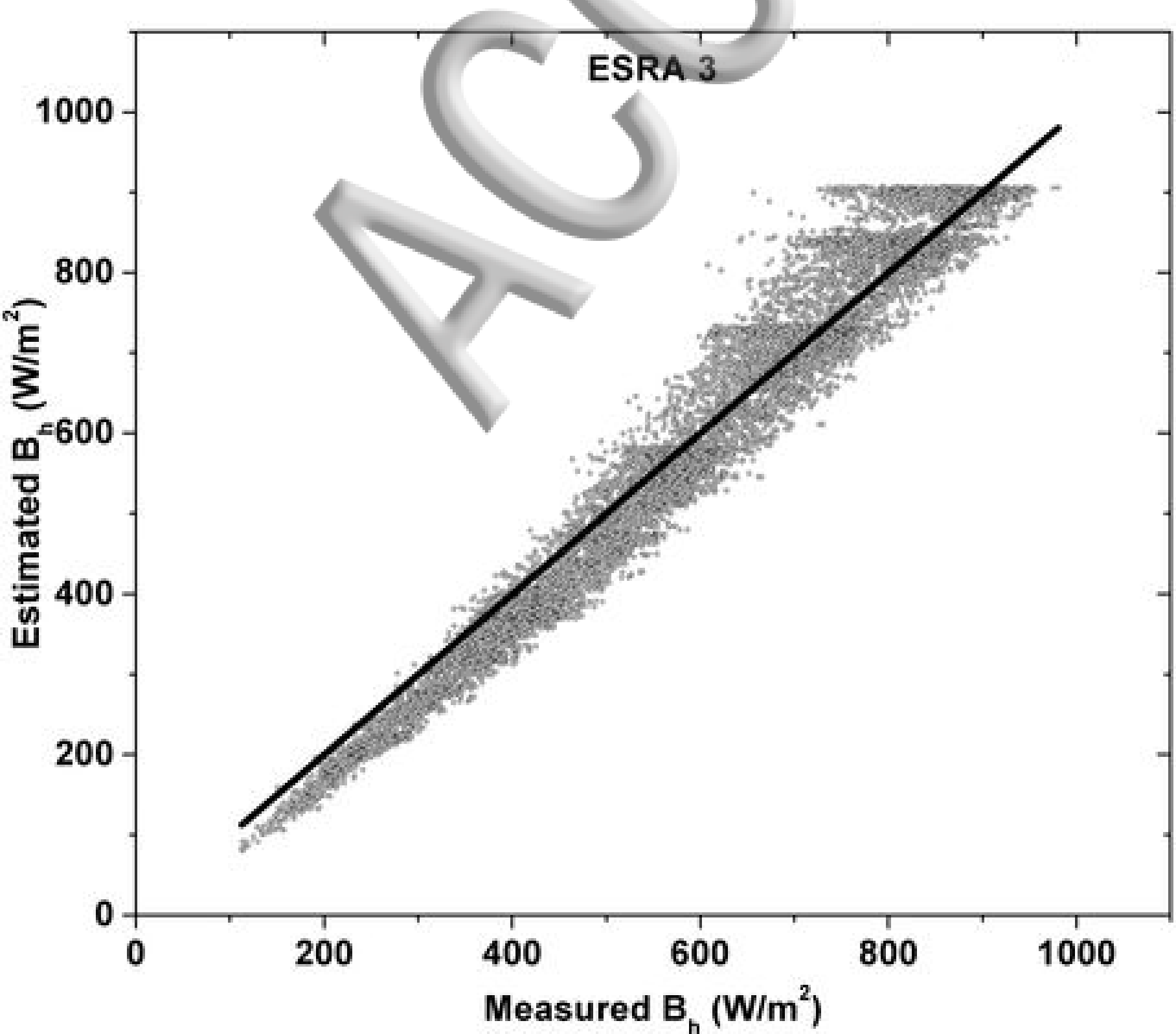
ESRA 3
1000
800
600
400
200
0
0
200
400
600
800
1000
Estimated B_h (W/m^2)
Measured B_h (W/m^2)